Chemical Engineering Science (2013). 93, 181-196.
DOI: http://dx.doi.org/10.1016/j.ces.2013.01.056

A definitive version was subsequently published in Chemical Engineering Science 93 (2013) pp. 181-196
doi:10.1016/j.ces.2013.01.056

Characterization of flow-induced vibrations in gas-solid fluidized beds: elements of the theory

Javier Villa Briongos*, Celia Sobrino, Jesús Gómez-Hernández, Domingo Santana

Universidad Carlos III de Madrid. Escuela Politécnica Superior. Departamento de Ingeniería Térmica y de Fluidos, Avenida de la Universidad 30, 28911, Leganés (Madrid)

*Correspondence to the author, e-mail: jvilla@ing.uc3m.es

Abstract:

This paper revisits the basic hypothesis underlying the measurement of flow-induced vibration in fluidized beds. A novel theoretical approach based on the standing pressure field characterizing the bed dynamics is proposed to link the pressure fluctuations to the measured accelerometer signals. The model provides a reliable prediction of the carrying frequency band and helps in designing the accelerometer measurement process. The model was tested with previous results reported in the literature as well as with piezoelectric accelerometer measurements collected from a lab-scale experimental facility. A study on accelerometer measurements was conducted to identify the main limitations expected for measuring flow-induced vibrations in a gas-solid fluidized bed. The structural response of the vessel to flow-induced vibration was mostly determined by the "bed acoustics" that can be dominated by either elastic or compression waves. Finally, the survival of an envelope process on the measured accelerometer signal guaranteed the quality of the flow dynamical information collected during the measurement process.

Keywords: Fluidization; Design; Instrumentation; Vibration analysis; Hydrodynamics; Control

1. Introduction

The increasing need for non-invasive measurement methods for the monitoring of gas-solid fluidized beds (FB's) prompted the use of the so-called „acoustic' monitoring (AE) methods (Boyd and Varley, 2001;Briens and Bojarra, 2010;Cents et al., 2004;Tsujimoto et al., 2000)(Tsujimoto et al., 2000; Boyd and Varley, 2001; Cents et al., 2004 Briongos et al., 2006; Briens and Bojarra, 2010). By providing measurements that do not interfere with the bed dynamics, these promising techniques using both acoustic (sound waves) and vibration measurements (structural waves) offer several advantages with respect to the measurement techniques that use invasive methods. Although sound pressure waves and flow-induced vibrations possess distinct features, most of the reported literature does not distinguish between sound waves propagating through an elastic fluid medium and vibration waves circulating across structural elements. The measured sound and solid waves are all referred to as AE signals, even for the sound waves measured using microphone devices with the vibration motion mostly collected through accelerometer transducers. The wave motion exhibited by both types of measured signals explains the direct analogy historically established between the sound and the structural vibration waves. Understanding the fundamentals of sound and structural waves prior to addressing the flow-induced vibration problem is necessary by taking into account the results of the propagating waves through a fluid medium, as the sound waves can only store energy in compression (longitudinal waves). For the circulation through a solid material, both shear and compression components can store energy, giving rise to longitudinal, flexural and torsional waves. The measured vibration signal accounts for shear as well as the compression terms.

Among the different measurement techniques included within the „AE' methods, the monitoring of mechanical vibrations using accelerometer transducers is currently receiving considerable attention (He et al., 2009;Leskinen et al., 2010;Wang et al., 2009;Wang et al., 2010). To monitor the performance of a specific fluidized bed application, these previous works typically used the accelerometers to gather knowledge on the so-called fluidization quality. Consequently, the accelerometer measurements have been successfully applied in granulation processes to detect agglomeration phenomena or to measure bed fluidity (Book et al., 2011). Accelerometers can also be used to assess the behavior of specific fluidized bed operations, such as the liquid injection process in gas-solid fluidized beds (Briens et al., 2011). Fluidized bed

dynamics have also been studied with vibration measurements using accelerometers (Abbasi et al., 2010;Cody et al., 1996).

Though never explicitly mentioned, the hypothesis underlying the use of accelerometer transducers is based on the assumption that the measured signal corresponds to the flow-induced vibrations originating from the FB dynamics. In spite of the extensive literature concerning accelerometer measurements, a theoretical framework on the flow-induced vibrations in gas-solid fluidized beds is still needed to further understand the measured accelerometer signals and to guide the design of the measurement process. For the sampling frequencies used to collect the accelerometer signals, two very different measurement approaches have been used in the literature to address the measurement of the accelerometer signals in gas-solid FB's. One type of measurement method in the ultrasonic ranges used sampling frequencies of the order of hundreds of kHz (Cao et al., 2009;Tsujimoto et al., 2000). These „high frequency' studies assumed that the „acoustic emission' (i.e. flow induced vibration) resulted from the particle-particle and particle-wall collisions, suggesting that an "impact model" can account for the elastic waves resulting from these particle collisions. These methods should have provided a reliable estimation of the carrier frequency component of the measured accelerometer signal for measurements in the ultrasonic range (Jiang et al., 2007). One of the main drawbacks of this approach results from the high computational cost of sampling at those high frequencies, as the great number of data in each sample complicates the measurement process, limiting the number of time series analysis techniques that can be used to handle the data. A more commercial low-cost measurement approach has been developed that uses sampling frequencies that are considerably reduced in the measurement ranges between 20 kHz to 50 kHz (Abbasi et al., 2010;Abbasi et al., 2009;Cody et al., 1996;Cody et al., 2008). With this low frequency approach, two very different interpretations of the measured accelerometer signals are used to understand the flow-dynamic information of the FB system. In (Cody et al., 1996), the measured mechanical vibrations were also attributed to random particle impact. In contrast, (Abbasi et al., 2009) used the accelerometer measured signal to study bubble dynamics, assuming that the vibration signal recorded by the accelerometers „directly reflects the bubble characteristics'. For the accelerometer signal collected at high or low frequencies, the results reported in the literature suggest that these AE methods can be useful in extracting information on the fluidized bed dynamics. A major question arises on the compatibility of the different previously

reported approaches regarding the depth that an accelerometer signal analysis can provide to properly use the accelerometer signals.

For the AE measurements and, in particular, the use of accelerometers for measuring mechanical vibrations, several complications are expected during the measurement process (Vervloet et al., 2010). The fact that the measured accelerometer signals accounted for the dynamical response of the structure as well as for the FB dynamics suggests that the measured accelerometer signal can contain information of the unwanted structural motions (structure-borne sound) as well as other background noises and signal losses resulting from the structural and material dampening. These factors can obscure the flow dynamics information carried within the measured signal. The physical meaning of the so-called vibrating signals should not be ignored in understanding both the measured signals and the measurement process.

Recently, a close relationship between the acceleration and the pressure fluctuation signals measured simultaneously in a gas-solid fluidized bed operating at different fluidization conditions has been reported (de Martin et al., 2010), suggesting that further attention should be given to the study of the relationships between pressure fluctuations and flow-induced vibrations.

Within the framework of the well-known flow induced vibration theory, this paper presents a novel approach using a standing pressure field developed within the bed to link the pressure fluctuations resulting from the fluidized bed dynamics with the measured accelerometer signals. The model provides a reliable prediction of the carrying wave frequency and can be used to design the accelerometer measurement process, helping to understand how the FB dynamical information can be encoded within the accelerometer signals.

2. **Flow-induced vibration in fluidized beds**

The basic hypothesis underlying the measurement of „flow-induced vibrations' establishes that: *i*) the motion of the structure does not significantly influence the pressure on the surface of the structure; and *ii*) the flow is a stationary, ergodic „random process' (Blevins, 1986). To have reliable flow-dynamics measurements, both points *i* and *ii* should be satisfied for measurements of the flow dynamics using a vibration analysis. The „flow-induced vibration' reflects the surface pressure on a structure (due in this case to the FB dynamics) as a result of the interaction between the bed dynamics phenomena (i.e. bubble, bulk and particle dynamics) with the resonant bandwidth of the

structure. The flow-induced vibration is also strongly dependent on the experimental setup and the measurement process (McConnell, 1995).

For the design of the accelerometer measurement process for a certain fluidized bed application, knowledge of the carrying frequency band of the measured accelerometer signal is critical in defining the measurement set up and the subsequent monitoring conditions. As stated above, only a few examples can be found in the literature (Jiang et al., 2007;Leach et al., 1978) that provide information to generate some understanding of the carrier frequency band properties characterizing the measured accelerometer signal. These previous works mostly focused on the relationship between the particle characteristics and the measured acceleration signals. A model developed in (Jiang et al., 2007) based on the relationship between particle collisions and acoustic signals dealt with the measurement of the elastic waves produced by the particle-particle and particle-wall collisions. Consequently, the expected carrying resonant frequency band had considerably high frequency values, requiring the use of very high sampling frequencies ranging from 100 kHz to 500 kHz (Jiang et al., 2007;Tsujimoto et al., 2000). Even though several reports suggested that these high frequency methods can be tuned to serve for some fluidized bed applications, the sampling frequencies on the order of hundreds of kHz considerably can increase the computational costs needed to handle the monitoring problem. In addition, this approach disregards two important factors, such as the compression waves (van der Schaaf et al., 1998) and the structural vessel dynamics, which might affect the measurement of flow-induced vibration resulting from the fluidized bed dynamics, as discussed below. Consequently, the use of a theory based solely on “elastic waves” as the single source of „Acoustic Emissions (AE)’ cannot be easily extended to other FB systems and does not explain the most recent research results in the field (Abbasi et al., 2009;Cody et al., 1996;Cody et al., 2000;de Martin et al., 2010;de Martin et al., 2011;Li et al., 2011).

To analyze the relationship between the acoustic and vibration waves and to provide an increased understanding into the sound and vibration mechanisms responsible for the measured acceleration signals, a novel model is proposed to account for the interaction between both the acoustic pressure field (resulting from the elastic and compression pressure waves) and the vessel response. As shown below, the model links the standing pressure wave pattern resulting from the fluidized bed dynamics with the measured accelerometer signals.

A continuous system has an „infinite' number of natural frequencies, and a characterization of the „true' response spectra is not trivial (McConnell, 1995). The major issue regarding the design of the accelerometer measurement process is to develop a reliable prediction of the carrying frequency band that will carry the flow dynamic information. The proposed model is intended not to mimic the measured accelerometer signal but to predict the carrying frequency band to define both the accelerometer and the measurement conditions.

In the following sections, the pressure wave pattern developed within the bed is first discussed followed by a discrete approximation of the solution of the mechanical vibration of the vessel structure to link with the pressure field.

3. The pressure field

The origin and the propagation of pressure waves in fluidized beds have been the subject of substantial research efforts (Bi et al., 1995;Musmarra et al., 1995;Roy et al., 1990;van der Schaaf et al., 1998). The propagating pressure waves, which are mainly a result of the fluctuations in gas or particle velocities and to local changes in the bed voidage, are coupled with "forced fluidized bed oscillations", leading to an acoustic wave pattern characterized by a natural period of the pressure oscillation, t_n.

Previous results reported in the literature (Baskakov et al., 1986;Brown and Brue, 2001) demonstrated that bubbling fluidized beds might be explained by second-order dynamical systems. In Hao and Bi (2005), a second order dashpot model was proposed to explain the pressure fluctuations in gas-solid fluidized beds, demonstrating that the response of the pressure fluctuations originated in the bed due to a periodic driven force was adequately explained by the proposed model by setting the „zero' frequency, f_0, of the model as:

$$f_0 \sim \sqrt{g/H_{bed}} \tag{1}$$

For freely bubbling beds, the dominant frequency of the spectra was always larger than the characteristic frequency obtained from eq.1.

Purely periodic oscillations of the gas pressure in gas-solid fluidized bed described by expressions analogous to eq.1 have been observed in shallow beds (Verloop and Heertjes, 1974). As noted in Hao and Bi (2005), the different dynamical forces acting within a freely fluidized bed (i.e. bubbles) might force the characteristic oscillation towards frequencies greater than this zero frequency, f_0. Consequently, the natural

period of oscillation of the pressure wave propagation will be characterized by the frequency of a stationary „resonance state'.

Different theories addressed the characterization of this „natural period'. Among these theories, the approaches followed independently by (Roy et al., 1990) and (Herrera et al., 2002) are based on the propagation of plane waves in tubes of finite length (Billingham and King, 2000). These theories led to the use of two different expressions that yield a value of the natural frequency, f_n, that provides a reliable prediction of the measured resonant frequency data. As reported in Roy et al. (1990), the bed is modeled as a compressible pseudo-homogeneous gas-solid mixture without the relative motion and the interactions between the particle and the gas phases, leading to the following expression for t_n:

$$\frac{1}{f_n} = t_n = \frac{4H_{bed}}{c_s} = \frac{4H_{bed}}{c_{s0}} \sqrt{\frac{\gamma\varepsilon\left(\rho_p(1-\varepsilon)+\rho_g\varepsilon\right)}{\rho_g}} \tag{2}$$

A pseudo-homogeneous model can be used to estimate the pressure wave propagation velocity, c_s. In contrast with the approach followed in Herrera et al. (2002), the bed is treated as a single homogeneous medium with the use of a known solution for the natural frequencies of the gas oscillations in a tube of length H_{bed} closed at one end:

$$\frac{1}{f_n} = t_n = \frac{4H_{bed}}{c_s} \cdot \frac{1}{(2m-1)} \tag{3}$$

where c_s can be experimentally estimated from the corresponding standing wave pattern, assuming a rigid distributor, which results in an application of the separated-flow compressible-wave theory to the problem. The natural frequencies computed from either the pseudo-homogeneous or the separated flow approaches are approximately of the same order as the first mode of eq. 3, $m = 1$.

To characterize the pressure wave pattern that identifies the fluidized bed dynamics, both the pseudo-homogeneous and the separated flow approaches are valid for the acoustic fields controlled by the compression waves. These conditions are consistent with the experimental observations reported in the literature, apparently confirming that the propagation wave velocities can be well predicted by both approaches. The separated flow theory has been reported to be more appropriate in accounting for c_s with the observed effects of the wave frequency and the particle size (i.e. elastic waves) (Bi et al., 1995;van der Schaaf et al., 1998). In this paper, the separated-flow compressible-wave theory is used to characterize the natural frequency of the bed. The equation stated

below, reported in Ryzhkov and Tolmachev (1983), can be used to account for the pressure propagation wave velocities:

$$c_s = c_{s0}\sqrt{\frac{\rho_g}{\rho_p(1-\varepsilon)\varepsilon}\left(\frac{1+\omega^2\tau_p^2 B}{1+\omega^2\tau_p^2 B^2}\right)} \tag{4}$$

with the density ratio and the particle relaxation time defined, respectively, as:

$$B = \frac{\rho_g\varepsilon}{\rho_p(1-\varepsilon)+\rho_g\varepsilon};\ \tau_p = \frac{\rho_p d_p^2}{18\mu_g} \tag{5}$$

With both the angular wave frequency, ω, appearing in equation 4 and the propagation wave velocities needed to estimate the natural bed frequency in eq. 3 are unknown, an iterative approach using a zero order conjugate gradient method routine can be used. The initial trial value for w used in eq. 3 was taken from the quarter of the period of the wave frequency estimated from the pseudo-homogeneous approach (eq. 2) (van der Schaaf et al., 1998), with the resulting c_s value used to compute a new natural period (eq. 2) and so on. No more than three iterations were needed to converge. For a first trial, the natural frequency of the bed can also be roughly estimated using eq. 2 with a pseudo-homogeneous model to account for the pressure wave velocity.

4. The structural response

To link the acoustic (pressure) emissions resulting from the bed dynamics phenomena with the measured accelerometer signals, the resonant bandwidth of the structure must be identified to determine where the dynamical information will be carried. A relatively simple method to solve the complex vibration problem of a continuous system breaks the distributed inertia of the continuous system into a finite number of lumped inertia elements (nodes). A discrete approximation of the solution of the mechanical vibration of the vessel structure, which is considered to be a multidegree of freedom system (MDOF), can be used to represent the flexural (bending) vibration of the vessel structure.

For the exact determination of the natural frequencies from a continuous model, the discrete approach also requires the solution of a matrix eigenvalue problem. In this line, an evaluation of the stiffness influence coefficients is a common practice in the structural analysis for solving the different vibration modes of a given MDOF problem (Clough and Penzien, 2003). For mechanical systems, the calculation of stiffness

influence coefficients for a MDOF having n nodes requires the solution of n simultaneous equations, which might lead to a significant computational effort for systems characterized by many degrees of freedom. In contrast, the use of flexibility influence coefficients, f_{ij}, defined as the deflection of the coordinate node i due to a unit load applied to node j, provides a simple way to deal with the problem. As these influence coefficients are defined as the inverse of the stiffness matrix, knowledge of these values is sufficient for solving a free vibration problem, providing the natural frequencies and the mode shapes of the fluidized bed vessel structure (Appendix I).

The transient response of the structure to force excitations

The natural frequencies and mode shapes play a vital role in the vibration of the structure, and the knowledge of the undamped response of a MDOF system provides a first glance of the resulting accelerometer spectra. Real systems are damped and the analysis of the response of the structure under given excitation conditions becomes critical in understanding the modal characteristics of the vessel structure.

During the analysis of the dynamic response of a MDOF system, the displacement mode superposition approach leads to the following governing equation (Gatti and Ferrari, 2003):

$$M_n\ddot{X} + C_n\dot{X} + K_nX = f(t) \tag{6}$$

where the M_n, C_n, and K_n terms account, respectively, for the mass, damping and stiffness matrices, with $f(t)$ representing a time dependent one-dimensional vector of the forcing functions (Table 1). M is a diagonal matrix whose diagonal elements are the nodal masses, m_i, and the stiffness matrix obtained from the inverse of the flexibility matrix (Appendix I). Using theory (McConnell, 1995) as a first approximation, a viscous damping model can be assumed, and the damping coefficient matrix C_n, can be expressed as a function of the modal damping factor, ξ_n, as:

$$C_n = 2\xi_n w_n M_n \tag{7}$$

The natural frequencies of the mode shapes, w_n, can be estimated with the flexibility matrix approach (Appendix I), and the damping factor can be determined experimentally or estimated theoretically. As presented below within the acoustic interaction model section, this study is restricted to the modal expansion of the subset of n-modes obtained from the acoustic interaction model (following the mode

displacement method). The choice of the number of nodes, *n*, taken into account during the simulations is critical to obtain an accurate solution. For arbitrary viscous damping, the modal matrix does not diagonalize the damping matrix, and the system expressed in eq. 5 can be solved in state space using a discrete-time transition matrix approach (de Silva, 2000). The state response of the system can be expressed as a function of the state transition matrix. Accordingly, the state and the input vector are defined as:

$$x = \begin{bmatrix} X \\ \dot{X} \end{bmatrix}; u = f(t) \tag{8}$$

To obtain the measured acceleration response of the system, equation 5 can be rewritten as follows:

$$\ddot{X} = -M_n^{-1}K_n X - M_n^{-1}C_n \dot{X} + M_n^{-1} f(t) \tag{9}$$

Combined with the "identity, $\dot{X} = \dot{X}$", this expression can be put into matrix notation as:

$$\begin{bmatrix} \dot{X} \\ \ddot{X} \end{bmatrix} = \begin{bmatrix} 0 & I \\ -M^{-1}K & -M^{-1}C \end{bmatrix} \begin{bmatrix} X \\ \dot{X} \end{bmatrix} + \begin{bmatrix} 0 \\ M^{-1} \end{bmatrix} f(t) \tag{10}$$

Next, eq. 9 can be written in state space form:

$$[\dot{x}] = Ax + Gf(t) \tag{11}$$

The temporal evolution of eq.10 can be determined using the Laplace transform method. The solution is then given as a function of the state transition matrix, *Φ(t)*, as:

$$x(t) = \Phi(t)x(0) + \int_0^t \Phi(t,\tau)Gf(\tau)d\tau \tag{12}$$

where the first and the second terms on the right-hand side of eq.11 account, respectively, for the „free' and the „forced' state responses of the system. The state transition matrix, *Φ(t)*, is given by the matrix exponential expansion equation:

$$\Phi(t) = e^{At} = I + At + \frac{1}{2!}A^2t^2 + \ldots \tag{13}$$

Φ(t, τ) represents the time series obtained from eq. 12 by replacing *t* by *t-τ*:

$$\Phi(t,\tau) = e^{A(t-\tau)} \tag{14}$$

5. The acoustic interaction model

A continuous system has an „infinite' number of natural frequencies. To estimate the structural response of the fluidized bed vessel through the flexibility matrix approach, a suitable number of nodes is necessary to avoid the so-called spatial aliasing problem, as the mode shape that can be adequately described through the proposed discrete approach depends on the number of nodes used to describe the system. The linear constraints imposed by the normal-mode solution approach used to described the structural response implies that each natural frequency obtained from the reciprocals of the positive squared roots of the eigenvalues of the flexibility matrix has at least one corresponding mode shape, which should be represented by an homogeneous 2^{nd} order linear equation (eq. 6). The existing analogy between the form of the solution used to describe both the pressure field and the structural response is the departure point to propose an interaction model between the pressure and the structural problems to set a suitable number of nodes.

The mode shapes responsible for the different normal modes of vibration of the vessel structure are proposed to be directly related to the stationary wave pattern characterizing a freely bubbling bed. As shown in Figure 1, the number of nodes per unit length needed to perform the discrete lumped approximation to the continuous vessel is directly linked with the mode shape excited by the natural bed frequency characterizing the pressure wave pattern of the fluidized bed system, which, as stated above, is estimated with eq. 3.

The departure hypothesis of the acoustic interaction model assumes that:

1. The natural bed frequency estimated with eq. 3 is seen as a resonance state of the „zero' bed frequency, f_0, computed from eq. 1.
2. The pressure waves propagate at c_s.
3. The wavelengths are interpreted as the distance between beats („pulses') over the structure. The wavelength corresponding to the purely periodic oscillations (zero state), λ_0, is taken as the reference length.
4. The fluidized bed is treated as a one degree „damped' vibration system characterized by a natural frequency, f_n, resulting from the „resonant effect' that the different excitation forces appearing in a freely bubbling bed have over the „zero' bed frequency, f_0.

The number of nodes, n, is given as the ratio between the wavelengths characterizing, respectively, the „zero' and the resonance states:

$$n = round\left(\frac{\lambda_0}{\lambda_n}\right) \Rightarrow round\left(\frac{c_s/2\pi f_0}{c_s/2\pi f_n}\right) \Rightarrow round\left(\frac{f_n}{f_0}\right) \tag{15}$$

As depicted in Figure 1, for the natural frequency characterizing the bubbling fluidized beds equaling the zero frequency that characterizes the purely periodic oscillations, the number of nodes will be one. Larger natural frequencies than the zero frequency give rise to the number of nodes. As shown in Figure 1, some damping effects are included in f_0, as estimated according to (Verloop and Heertjes, 1974) as:

$$f_0 = \frac{1}{2\pi}\sqrt{\frac{g}{H_{bed}}\frac{1-\varepsilon}{\varepsilon}} \tag{16}$$

The minimum of number of nodes provided by eq. 15 should be used to avoid the spatial aliasing problem. The model given by eq. 12 should be solved by integrating the structural problem resulting from the partition of the continuous system into the corresponding nodes computed through eq. 15 to have a reliable structural response. Using a large number of nodes can result in an increased frequency resolution in the frequency domain with an increase in the computational cost with increasing the number of nodes.

In addition to the useful information generated to understand the measurement process provided by the model, from a design of the measurement process point of view, the acceleration data provided by the model can be properly sampled to match the experimental sampling frequency used during the acceleration measurements to assess the suitability of existing commercial accelerometers for specific applications.

6. Experimental.

To test the reliability of the proposed theory and to estimate the resonant bandwidth of the structure that will interact with the bed, the transient response of the model to several pulse-type excitation functions was investigated (Table 1). The sinusoidal type function was chosen to model the pressure excitation force applied by the fluidized bed dynamics on the vessel structure (Bi et al., 1995;Musmarra et al., 1995;Roy et al., 1990;van der Schaaf et al., 1998). This study shows how the boundary conditions and the measurement position can affect the resulting bandwidth spectra. The surrogate

accelerometer signals constructed using the measured pressure signals as forcing functions in eq. 6 were used to compare the resulting frequency spectra with the measured accelerometer signals collected during the present research.

Experimental Set-up

Pressure fluctuations and piezoelectric acceleration measurements were collected from a PMMA-gas-solid fluidized bed of 0.192 m ID with a bed aspect ratio of H/D = 0.75 (Table 2). The bed was operated with a 6 mm thick perforated plate distributor with 275 holes of 2 mm diameter distributed in a triangular arrangement with an 11 mm pitch. To prevent raining through the orifices, a wire mesh of 100 μm was placed below the distributor. Previous results reported in literature were used to validate the proposed model.

The accelerometry and pressure fluctuation signals were measured simultaneously for 4 minutes. A flow meter system consisting of a set of Cole-Parmer rotameters was used to control the air supply to provide bubbling regime conditions ($1.6 < U_r < 2.1$) using the operational conditions shown in Table 2.

Vibration measurement

The horizontal vibrations of the vessel wall were collected using two commercial accelerometers (Brüel and Kjaer Type 4507 B 005) located in the external face of the wall to account for the transversal vibrations of the vessel wall by the mounting slots supported with glue. The accelerometers were placed at 0.14 m and 0.07 m from the distributor, at the same height as the Kistler pressure transducer. The accelerometers were fitted to a NI 9233 (National Instruments) acquisition module mounted in a NI cDAQ-9172 system connected to a PC. The software used to acquire the signals was Labview 2010. The sensors had a sensitivity of 995 mV/g and a resonant frequency of 16.3 kHz. The sampling frequency was set to 10 kHz. Special care was taken with the wire that connects each accelerometer with the data acquisition device to avoid triboelectric noise in the signal.

Pressure fluctuation measurement

Pressure fluctuations were recorded by two probes placed at 0.14 m and 0.07 m height, respectively, and connected to a Kistler pressure transducer Type 7261. The transducers were connected to an adjustable range charge amplifier Type 5015. The charge

amplifier acted as a high-pass filter with a filter frequency of 0.1 Hz with only the fluctuating part of the signal recorded. The charge amplifiers were connected through a NI 9234 module to the cDAQ-9172 system. For the accelerometer system, the sampling frequency for the pressure fluctuations measurements was set to 10 kHz.

7. Results and discussion

7.1 The response spectra

For the measurement of the flow dynamics using a vibration analysis, the „flow-induced vibration', which reflected the surface pressure on a structure, is produced as a consequence of the interaction between the bed dynamics phenomena and the resonant bandwidth of the structure. Using a discrete approximation for the solution of the acoustic interaction on the vessel structure, the response of the vessel wall to the surface pressure induced by the fluidized bed dynamics is dependent on the force applied on each node (lumped inertia element) of the vessel structure. With the unsteady FB dynamics, the gas flow interactions generate pressure fluctuations within the corresponding standing wave pressure pattern, which result in a varying pressure field on the surface of the structure that might affect several „nodes' simultaneously. As a consequence, the spatial and frequency content of the pressure fluctuations might be influenced by the response spectra of the nearby nodes. The different conditions (fixed-free, pinned-pinned, fixed-pinned and fixed-fixed configurations) of the vessel boundary used during the computations might also change the spectral response of the vessel to the flow-induced vibrations (Table 1). The influence of these factors on the measurement process is explored below to set the criteria for the choice of the simulation settings to be used during the designing of the accelerometer measurement process. In real systems, the response spectra are far more complex, including multiple contributions, in addition to the transversal vibrations considered by the proposed model. These additional contributions can include rotational and base excitation contributions to the response spectra. As the continuous system has an „infinite' number of natural frequencies, understanding the response spectra can be a tricky problem.

7.2 Effect of boundary conditions

The boundary conditions can often be a source of error in the comparison of field and laboratory measurements, as small changes in a structure at a certain key point might

have an important effect on the “final boundary conditions”. The possible deviations between the field measurements and the predicted responses are essential to understand this system. As shown in Figure 2, the estimated normalized frequency response of the cylindrical UC3M vessel (Table 2) using a sinusoidal pulse-type excitation function are given for the four different boundary conditions (Table 1): fixed-free, pinned-pinned, fixed-pinned and fixed-fixed. Figure 2a shows the temporal response of the system to the sinusoidal input (Table 1). Two different spectrum types can be observed, depending on the boundary condition used. The fixed-fixed and fixed-free cases had very similar amplitude responses in the time domain. Within the frequency domain, the corresponding spectral energy was distributed over a band of frequencies having an energy magnitude roughly the same order of magnitude as the center frequency of the band. A confirmation of the field measurements with these two boundary conditions would be expected to produce a wide-band process characterized by frequencies ranging approximately from 500 Hz to 4500 Hz (Figure 2b). In contrast, the pinned-pinned and the fixed-pinned conditions were characterized by temporal responses with large amplitudes and narrow spectra in the frequency domain, with the center frequency having a larger magnitude than the rest of the characteristic frequencies appearing within the spectra. The band frequency responses characterized by a frequency centered around 3000 Hz and 2500 Hz for the pinned-pinned and the fixed-pinned, respectively, were predicted for the experimental facility matching the pinned-pinned or the fixed-pinned conditions. To assess the reliability of the proposed model to predict the carrying frequency band, the frequencies responses in Figure 2b were compared to the normalized Power Spectral Density (PSD) of the experimental accelerometer signal measured under bubbling operating conditions (Table 2).

Figure 3b shows the PSD function of the measured Brüel and Kjaer Type 4507 B 005 accelerometer signals collected at 10 kHz from the UC3M PMMA vessel (Table 2). The fluidized bed facility was fixed at the distributor extreme with the other extreme set free, matching the experimental fixed-free boundary configuration. To compare the experimental and simulated data, the PSD spectra should be dimensionless as the simulates data corresponded to the pulse-type excitation conditions whereas the experimental data accounted for the spectra of the current measured accelerometer signals. Both the content and the distribution of the energy were quite different in magnitude.

According to the literature, three different regions can be distinguished in the spectrum of Figure 3a: the mean response region that corresponds with the average displacement of the structure produced by the long term behavior of the vessel vibration, the non-resonant (buffeting) response region of the vessel at frequencies below the resonant bandwidth of the structure, and the resonant response region due to the vibration of the structure as a consequence of flow induced vibration within the resonant frequency band. The resonant region was characterized by a wide-band frequency signal ranging from 1000 Hz to 4000 Hz, as expected for the fixed-free boundary condition. Figure 3b shows the frequency response of the structure corresponding to the sinusoidal pulse-type excitation presented previously in Figure 2b for the fixed-free boundary conditions. The model predicted the broad band frequency content along the resonant response region. Without a mean flow excitation, the region resulting from the mean response of the structure did not contain a frequency component. The same low frequency content can be observed within the buffeting region, where only small frequency content was expected. The model provides a reliable prediction of both the type and the size of the resonant bandwidth of the structure.

7.3 Effect of distributed excitations and the measurement distance to the excitation point on the measured accelerometer signals.

The measured accelerometer signal can originate from the distributed and concentrated flow dynamics loads, resulting in the vibration of the structure within the mentioned resonant response region. For the measurements of the flow-induced vibration originating from the FB dynamics, the distributed loads can be related to the coherence phenomena, such as bubble coalescence, gas flow fluctuation, bubble eruption and bed mass oscillation, which generate fast pressure waves that can affect almost instantaneously the surface pressure above the vessel structure (Bi et al., 1995;Musmarra et al., 1995;Roy et al., 1990;van der Schaaf et al., 1998). In contrast, the concentrated flow-induced vibrations should account for the local fluctuations in pressure corresponding to low coherence phenomena, such as gas bubbles and turbulence. Regardless of whether the distributed or the concentrated loads are the forces responsible of the measured flow-induced vibrations, the theory of the vibrating testing states that the characterization of the response spectra of both the concentrated and the distributed loads should require the simultaneous measurement of the vibration motion at different locations to identify the structure mode shapes. Without this

consideration, the information from some significant modes can be missed (McConnell, 1995). The characterization of the „true' response spectra is not trivial. Previous studies that used *AE* methods for monitoring the fluidized beds dynamics reported the collection of accelerometer measurements at different locations of the structure (de Martin et al., 2010;Li et al., 2011), taking into account the influence of the measurement position on the measured signal. In de Martin et al. (2010), the accelerometer and pressure measurements collected at the different bed positions were used to study the coherence phenomena. A close relationship between the IOP and COP spectra was estimated from the pressure fluctuation measurements and the associated envelope process of the accelerometer signals. No conclusions have been made on the effect of the structural dynamic vessel responses on the measured signals.

The existing limitations in acquiring the „true' response spectra require a visualization, at least qualitatively, of the mode shape leaks effects on the measured accelerometer signal within the resonant response region. Figures 4 and 5 show the theoretical response as a function of the concentrated and distributed loads, respectively, along the vessel structure for a sinusoidal pulse-type excitation having fixed-free boundary conditions. The concentrated load simulation was performed by applying the forcing function at node 2 at a spacing of 0.07 *m,* as measured from the bed distributor (Figure 4). The distributed load pulse-type run was performed by forcing simultaneously the different nodes with the same sinusoidal pulse-type function (Figure 5). In both cases, the corresponding acceleration signal was measured at the different node positions ranging between 0.03 m < n < 1 m to characterize the resulting response spectra.

As observed in Figure 4, the frequencies characterizing the resonant response region to the concentrated load excitation only propagate through the adjoining nodes, as the resonant response region remains almost intact in the proximity of the excitation point. The local phenomena behind the concentrated excitation can only be measured near the flow dynamic load source. This local feature can also be observed for other boundary condition situations with a fixed condition that can be applied to some of the boundaries. For the time domain response of the excitation, the amplitude response of the measured acceleration signal increased with the distance to the load point. This increase in the amplitude corresponded with an increase in the low frequency content appearing in the mean response and the nonresonant response regions. The flow dynamic information encoded within the resonant bandwidth region of the corresponding acceleration signals could have been masked with this response.

The effect of distributed loads for the fixed-free BC case, shown in Figure 5, or the other BC conditions suggested that the distributed load can propagate through the vessel by enhancing the low-frequency component of the acceleration signals. As a result of the distributed load effect, the center frequency characterizing the resonant frequency band was expected to be drawn to the low frequencies values.

These preliminary results indicated a different structural behavior for the local and global structural flow dynamics loads. Consequently, as for the pressure fluctuation measurements, the analysis of the accelerometer signals can be used to study both local and global phenomena.

7.4 Model testing.

To test the reliability of the proposed acoustic interaction theory in the study of the carrying resonant response region, several literature reports that cover the different approximations to the problem of flow induced vibration measurement in FB's were used for a comparison. The experimental conditions shown in table 2 were used to run the model for a comparison with the corresponding literature data.

The results obtained from the vibration induced by pulse-type excitation were used to demonstrate that the model performance predicted the carrying wave frequency band. The potential use during the subsequent design of the accelerometer measurement process is also discussed. A practical example of the vibration induced by the pressure time series excitation was presented to demonstrate the existing relationship between the acoustic and vibrations waves resulting from the pressure waves originating within the bed. The relationship between the pressure and the vibrations contribute to an understanding of the FB dynamical information that can be encoded within the measured accelerometry signals.

7.4.1 Vibration induced by pulse-type excitation

Figure 6 shows a comparison between the PSD of the simulated accelerometer time series obtained with fixed-fixed boundary conditions (dotted line) and the PSD of the experimental accelerometer signal, reported in (Cody et al., 1996) (solid line), for an aluminum vessel operating with glass spheres of d_p = 229 μm fluidized with helium gas (Table 2). As in Figure 3, the dimensionless spectrum was used in the comparison. Consistent with the results shown previously in Figure 3, the information regarding the mean response region of the vessel structure (low frequency region) was not taken into

account by the model. The PSD from the simulated time series exhibited a close behavior within the resonant response region. Within the resonance region, the flow dynamic information was carried by the FB dynamics. As shown in Figure 6, the model successfully predicted a complex wide-band response spectrum ranging from 1000 Hz to 20 kHz for measurements at 50 kHz (Table 2). This information is critical in guiding the design of the accelerometer measurement process. As discussed in the example shown below for the vibration induced by the pressure time series, this information may be used to assess the „quality' of the FB dynamic information contained in the measured accelerometer signal.

Figure 7 compares the PSD for the accelerometry signal collected from a PMMA laboratory-scale reactor reported in the literature (Jiang et al., 2007) (solid line) with the corresponding simulation runs obtained by a sinusoidal pulse-type excitation for the four different boundary conditions (dotted line). As stated above, the corresponding experimental results consider the elastic waves to be the single source of the measured accelerometer signals. Regardless of the boundary condition used, the model produced a reliable prediction of the measured resonant response region, with the center frequency value of the experimental and simulated spectra exhibiting a close agreement. The apparent independence of the predicted band response on the model boundary conditions was a result of the height of the bed ($H_b \sim 0.05\ m$) being very small, suggesting that the elastic waves produced by the particle-particle and the particle-wall collisions dominated the propagation velocity term ($f_n = 208\ Hz$, $c_s = 52\ m/s$) of the pressure field. Tall fluidized beds produced differing responses that suggested the importance of the compression wave term in these responses.

In spite of the great differences with the sampling frequencies chosen to measure the accelerometer signals (Table 2), both approaches reported in Cody et al. (1996) and Jiang et al. (2007) assumed that the particle-particle and particle-wall collisions were the single sources for the measured "Acoustic Emissions". This apparent inconsistency disappeared within the present approach, with the existing pressure wave pattern dominated by either the compression or the elastic waves.

To conclude with the validation of the vibration induced by the pulse-type excitation test, figure 8 compares the results reported in Abbasi et al. (2009). For the different fluidization conditions, the resulting PSD functions from the simulation runs exhibited a characteristic frequency peak close to the 1 kHz value (peak number one), which

characterizes the measured spectra. With the exception of the spectrum shown in figure 8b, the characteristic frequencies were always below 8 kHz, as reported in Abbasi et al. (2009). In addition, a secondary peak centered at approximately 4 kHz appeared in most of the simulated runs (peak number 2), which also appeared in the experimental signal for the H/D = 1 conditions (figure 8c).

Several comments on the results shown in figure 8 may be of interest. The fluidized bed facility used in Abbasi et al. (2009) had a circulating structure. The vessel's actual structural response cannot be modeled as a „single' beam due to the effect that the downcomer tube might have had on the boundary conditions. To use the single beam structural approach in the design of the accelerometer measurement process also in the circulating systems, a conceptual reduction of the current structural problem was needed to define a „single beam' problem that could be handled by the proposed simplified approach. As shown in Table 2, the column height, L, used in the model through the simulation, $L = 0.3\ m$, did not correspond with the experimental value of the vessel length, $L_{column} = 2\ m$, reported in the literature (Abbasi et al., 2009). To reduce the structural problem to a single beam problem, the vessel length used to compute the nodes in the calculations was roughly taken as the difference between the actual vessel length minus the downcomer length ($L = L_{column} - L_D$). Without these approximations, the actual vessel height was used through the computation, producing slight differences in both the response type and center frequency spectrum. For $L_{cal} = L = 2\ m$, the model predicted a wide carrier frequency band centered around 2 kHz, with the model overestimating the carrying wave and failing to predict the apparent narrow band process reported in literature. The model still predicted the lack of frequencies found above 8 KHz, which is also useful information for the design of the measurement process. A reliable prediction of both the center spectral frequency and the response type spectrum can be made after reducing the structural problem.

7.4.2 Vibration induced by a pressure time series

With the validation of the prediction for the expected carrying wave frequency band by a pulse-type excitation test to help the design of the accelerometer measurement process, a practical example of vibration induced by a pressure time series excitation was developed and presented below. This example illustrates the existing relationship

between the pressure field characterizing the FB dynamics and the signals measured by the accelerometers.

Recent literature regarding accelerometer monitoring (de Martin et al., 2010;de Martin et al., 2011;Li et al., 2011) has revealed the existing relationship between pressure fluctuations and accelerometer signals measured simultaneously from FB's. The low frequency information carried in the associated envelope process within the accelerometer signals can be directly related to the conventional pressure fluctuation measurements for the slow varying envelope conditions for the measured accelerometer signals (Langley, 1986). This approach is in agreement with the theory of random vibrations (Crandall and Mark, 1963), as the flow-induced vibrations should typically have a modulated response. In the FB system, this modulation might be produced by the interaction of the bed dynamics phenomena (i.e. bubble, bulk and particle dynamics) with the resonant bandwidth of the structure.

A vibration induced by a measured pressure time signals test was conducted to develop an understanding on the effects of the FB dynamics on the measured accelerometer signal as a consequence of its interaction with the resonant bandwidth of the structure. To facilitate these measurements, the pressure signals collected by the Kistler Type 7261 transducers at the UC3M FB facility (Table 2) were used as the forcing function, $f(t)$, of the structural model (eq. 5).

Figure 9a shows a comparison in the time domain between the measured and the simulated accelerometer signal provided by the model. The model described the quantitative and qualitative behavior of the experimental accelerometer signal. As the model produced a good prediction of the carrying wave frequency band, a close look at the time domain information of the signal depicted in Figure 9a revealed that the scales, t_m and t_e, characterizing the time domain information of the experimental signal can be found within the simulated acceleration signal (Figure 9b). The frequency domain analysis of both experimental and simulation signals (Figure 10) confirmed the reliability of the model to predict the expected carrying wave frequency band for the structural model forced with an experimental pressure time series. Figure 10a shows how the model predicted that the flow dynamic information would be carried within a wide carrying frequency band located within the resonant response region of the spectra (Figure 10b). Moreover as in the previous case, for the vibration induced by the pulse-

type tests, the model did not account for the information carried within the mean and the nonresonant response regions (Figure 3).

Figure 11 shows the PSD of the envelope signals from both the measured (dotted red line) and the simulation accelerometer signals (dotted black line). The Hilbert transform method reported in de Martin et al. (2010) was applied to extract the associated envelope processes. To compare the information carried by the experimental and the simulated envelope signals, the corresponding pressure time series measured at the same position of the acceleration signal is shown in Figure 11 (solid red line) (these pressure signals were used in eq. 5 to force the structural model). As expected, the relationship between the measured pressure signal and the envelope signal recovered from the measured accelerometer signal was apparent and in agreement with the results reported previously (de Martin et al., 2010). Only small differences can be observed between the corresponding PSDs at the low frequency region. To compare the pressure fluctuation measurements with the envelope recovered from the simulated accelerometer signal, a close agreement existed between the envelope and the pressure time series from 2 to 8 Hz. As shown in figure 11, a comparison for U_r = 1.6, which as a consequence that the corresponding fluidization regime is not yet well developed, produced the most unfavorable case between the simulated envelope process and the corresponding pressure fluctuation time series, focusing on the FB dynamics carried in the envelope process and not on the precise matching of the spectra. The structural response of the vessel to a flow-induced vibration was mostly determined by the "bed acoustics" estimated using the settle bed conditions. With the fluidization regime driving the envelope process, the distinct features characterizing the standing wave pattern at several fluidization conditions cannot be matched.

For the experimental accelerometer signal, a clear difference at the low portion of the PSD was observed between the envelope process associated with the simulated acceleration signal and the experimental pressure fluctuation signal used as a forcing function (please note the energy of the characteristic peaks appearing below 1.8 Hz in Figure 11). These differences appearing at low frequencies helped to identify unambiguously the origin of the dissimilarities as structural-born.

As the measured pressure time series used to force the structural model can be recovered from the envelope process, the envelope process was determined to account for the flow-dynamic forces behind the vibration of the structure, whereas the measured

accelerometer signals accounted for the dynamical response of the structure, which can also contain information of the unwanted structural motion as well as other background noises. Consequently, if the measured accelerometer signals are induced by the flow-dynamics of the fluidized bed, they might exhibit enough sensitivity to certain flow changes to appreciate some particular phenomena under study, explaining why the previous approaches dealing with accelerometer measurements gave acceptable outcomes for certain monitoring and control issues. The structural as well as the background noises can reduce the „quality' of the measured accelerometer signal, preventing an adequate application with this approach for multiple conditions, such as a detailed analysis of the dynamical processes (bubbles and particle dynamics) characterizing the dynamics of gas-solid fluidized bed.

8. Conclusions

The acoustic interaction model produced a reliable prediction of the carrying wave frequency at the different measurement sampling conditions that might be used by the outlined acquisition systems. The results provided by the vibration induced by the pulse-type excitation tests sufficed for these designing purposes. Several fluidization parameters, such as the fluidization velocity U_0, were not used to characterize the pressure field in the bed. Consequently, the structural responses of the vessel to flow-induced vibrations were mostly determined by the "bed acoustics". From the vibration induced by a pressure time series, the fluidization regime drove the envelope process. More research is needed to gain knowledge on the flow-induced vibrations in gas-solid fluidized beds.

The vibration induced by pressure time series excitation tests revealed a close relationship between the pressure fluctuation characterizing the FB dynamics and the flow-induced accelerometer signals measured simultaneously in the bed. This observation is in agreement with the most recent advances reported in the literature on this subject. The pressure time series excitation tests helped to understand the effects of the FB dynamical information on the measured signals. It can be used to discriminate between the contribution of both the flow dynamic information and the structural-born noise on the accelerometer signals collected from a FB system at the corresponding measurement conditions.

The mechanical response of the vessel to concentrating load excitation propagates through the adjoining nodes. Consequently, the local phenomena behind the excitation can only be measured near the flow dynamic origin of the load. In contrast, the distributed load can propagate through the vessel by enhancing the low-frequency component of the measured acceleration signals, bringing the center frequency characterizing the resonant frequency band to low frequencies values. This information is extremely important in dealing with the different phenomena behind the flow dynamic forces characterizing the fluidized beds and in placing the accelerometer for reliable monitoring.

As expected, the results shown through the paper confirmed that the measured accelerometer signal will be contaminated by unwanted structural motion. Consistent with the random vibration theory, the simulated accelerometer signal induced by an experimental pressure time series produced a modulated response as a consequence of the interaction of the bed dynamics phenomena with the resonant bandwidth of the structure. The simulated acceleration signal and the corresponding associated envelope process accounted for the different dynamics. The envelope time series accounted for the flow-dynamic forces behind the vibration of the structure (beating phenomena) and the measured accelerometer signals accounted for the dynamical response of the structure. The survival of an envelope process on the measured accelerometry signal guaranteed the quality of the dynamical information collected during the measurement process.

Notation

Uppercase letters

A_{cv}	cross sectional area of the vessel, m^2
B	density ratio, [-]
D	Internal bed diameter, *m*
E	Young Modulus of vessel material, *Pa*
F_0	Force magnitude, *N*
H	bed height, *m*
I	area moment of inertia, m^4
ID	Internal vessel diameter, *m*
L	vessel length, *m*

OD	external vessel diameter, *m*
U_r	reduced velocity $U_r = U_0/U_{mf}$, [-]
X	displacement vector, (mode shape), *m*

Lowercase letters

c_{s0}	pressure wave air propagation velocity, *m/*
c_s	pressure wave bed propagation velocity, *m/s*
d_p	particle diameter, *m*
f_0	natural „zero' frequency, *Hz*
f_n	natural frequency, *Hz*
g	acceleration of gravity, m/s^2
m_i	lumped mass, *kg*
m_v	vessel mass, *kg*
n	number of nodes per unit length, [-]
t_0	time rise for pulse time excitation
t_e	characteristic time of experimental accelerometry signal, s
t_m	characteristic time of simulated accelerometry signal, s
t_n	natural period of pressure oscillation, *s*

Greek letters

ω	angular frequency, *rad/s*
γ	*cp/cv* ratio, [-]
ε	void fraction, [-]
ε_{mf}	void fraction at minimum fluidization velocity, [-]
μ_g	dynamic viscosity of gas fluidizing gas, Pa·s
ρ_g	gas density, kg/m^3
τ_p	particle relaxation time, *s*
ρ_s	particle density, kg/m^3
ϕ_s	sphericity factor, [-]

Abbreviations

BC	Boundary condition.
CE	Cumulative energy PSD function
FB	fluidized bed

PSD Power spectral density

Acknowledgments

The author would like to thank the financial support from projects DPI2009-10518 (MICINN) and CARDENER-CM (S2009ENE-1660).

References

Abbasi, A., Sotudeh-Gharebagh, R., Mostoufi, N., Zarghami, R., Mahjoob, M. J., 2010. Nonintrusive Characterization of Fluidized Bed Hydrodynamics Using Vibration Signature Analysis, AICHE Journal 56(3), 597-603.

Abbasi, M., Sotudeh-Gharebagh, R., Mostoufi, N., Mahjoob, M. J., 2009. Non-intrusive monitoring of bubbles in a gas-solid fluidized bed using vibration signature analysis, Powder Technology , 278-85.

Baskakov, A. P., Tuponogov, V. G., Filippovsky, N. F., 1986. A Study of Pressure-Fluctuations in a Bubbling Fluidized-Bed, Powder Technology 45(2), 113-117.

Bi, H. T., Grace, J. R., Zhu, J., 1995. Propagation of Pressure Waves and Forced-Oscillations in Gas-Solid Fluidized-Beds and their Influence on Diagnostics of Local Hydrodynamics, Powder Technology 82(3), 239-253.

Billingham, J., King, A. C., 2000. Wave Motion. Cambridge, United Kingdom: Cambridge University Press.

Blevins, R. D., 1986. Flow-Induced Vibration. Malabar, Florida: Robert E. Krieger Publising Company.

Book, G., Albion, K., Briens, L., Briens, C., Berruti, F., 2011. On-line detection of bed fluidity in gas-solid fluidized beds with liquid injection by passive acoustic and vibrometric methods, Powder Technology 205(1-3), 126-136.

Boyd, J. W. R., Varley, J., 2001. The uses of passive measurement of acoustic emissions from chemical engineering processes, Chemical Engineering Science 56(5), 1749-1767.

Briens, L., Bojarra, M., 2010. Monitoring Fluidized Bed Drying of Pharmaceutical Granules, Aaps Pharmscitech 11(4), 1612-1618.

Briens, L., Book, G., Albion, K., Briens, C., Berruti, F., 2011. Evaluation of the Spray Stability on Liquid Injection in Gas-Solid Fluidized Beds by Passive Vibrometric Methods, Canadian Journal of Chemical Engineering 89(5).

Brown, R. C., Brue, E., 2001. Resolving dynamical features of fluidized beds from pressure fluctuations, Powder Technology 119(2-3), 68-80.

Cao, Y. J., Wang, J. D., Liu, W., Yang, Y. R., 2009. Wall sheeting diagnosis in fluidized beds based on chaos analysis of acoustic emission signals, Journal of Zhejiang University-Science a 10(9), 1341-1349.

Cents, A. H. G., Brilman, D. W. F., Versteeg, G. F., Wijnstra, P. J., Regtien, P. P. L., 2004. Measuring bubble, drop and particle sizes in multiphase systems with ultrasound, AICHE Journal 50(11), 2750-2762.

Clough, R. W., Penzien, J., 2003. Dynamics of Structures. USA: Computers and Structures, Inc.

Cody, G. D., Bellows, R. J., Goldfarb, D. J., Wolf, H. A., Storch, G. V., 2000. A novel non-intrusive probe of particle motion and gas generation in the feed injection zone of the feed riser of a fluidized bed catalytic cracking unit, Powder Technology 110(1-2), 128-142.

Cody, G. D., Goldfarb, D. J., Storch, G. V., Norris, A. N., 1996. Particle granular temperature in gas fluidized beds, Powder Technology 87(3), 211-232.

Cody, G. D., Johri, J., Goldfarb, D., 2008. Dependence of particle fluctuation velocity on gas flow, and particle diameter in gas fluidized beds for monodispersed spheres in the Geldart B and A fluidization regimes, Powder Technology 182(2), 146-170.

Crandall, S. H., Mark, W. D., 1963. Random Vibration in Mechanical Systems. Orlando, Florida: Academic Press, Inc.

de Martin, L., Briongos, J. V., Aragon, J. M., Palancar, M. C., 2010. Can low frequency accelerometry replace pressure measurements for monitoring gas-solid fluidized beds? Chemical Engineering Science 65(13), 4055-4064.

de Martin, L., Briongos, J. V., Garcia-Hernando, N., Aragon, J. M., 2011. Detecting regime transitions in gas-solid fluidized beds from low frequency accelerometry signals, Powder Technology 207(1-3), 104-112.

de Silva, C. W., 2000. Vibration: Fundamental and Practice. USA: CRC Press LLC.

Gatti, P. L., Ferrari, V., 2003. Applied Structural and Mechanical Vibrations: Theory, Methods and Measuring Instrumentation. London (UK): Taylor and Francis Group.

Hao, B. G., Bi, H. T., 2005. Forced bed mass oscillations in gas-solid fluidized beds, Powder Technology 149(2-3), 51-60.

He, Y. J., Wang, J. D., Cao, Y. J., Yang, Y. R., 2009. Resolution of Structure Characteristics of AE Signals in Multiphase Flow System-From Data to Information, AICHE Journal 55(10), 2563-2577.

Herrera, C. A., Levy, E. K., Ochs, J., 2002. Characteristics of acoustic standing waves in fluidized beds, AICHE Journal 48(3), 503-513.

Jiang, X. J., Wang, J. D., Jiang, B. B., Yang, Y., Hou, L. X., 2007. Study of the power spectrum of acoustic emission (AE) by accelerometers in fluidized beds, Industrial & Engineering Chemistry Research 46(21), 6904-6909.

Kelly, S. G., 1993. Fundamentals of Mechanical Vibrations. Singapore: Mc_Graw Hill, Inc.

Langley, R. S., 1986. On various Definitions of the Envelope of a Random Process, Journal of Sound and Vibration 105(3), 503-512.

Leach, M. F., Rubin, G. A., Williams, J. C., 1978. Analysis of gaussian size distribution of rigid particles from their acoustic emission, Powder Technol 19, 189-195.

Leskinen, J. T. T., Okkonen, M. A. H., Toiviainen, M. M., Poutiainen, S., Tenhunen, M., Teppola, P., Lappalainen, R., Ketolainen, J., Jarvinen, K., 2010. Labscale fluidized bed granulator instrumented with non-invasive process monitoring devices, Chemical Engineering Journal 164(2-3), 268-274.

Li, Y., Grace, J. R., Gopaluni, R. B., Bi, H. T., Lim, C. J., Ellis, N., 2011. Characterization of gas-solid fluidization: A comparative study of acoustic and pressure signals, Powder Technology 214, 200-210.

McConnell, K. G., 1995. Vibration Testing: Theory and Practice. USA: John Wiley and Sons, Inc.

Musmarra, D., Poletto, M., Vaccaro, S., Clift, R., 1995. Dynamic Waves in Fluidized-Beds, Powder Technology 82(3), 255-268.

Roy, R., Davidson, J. F., Tuponogov, V. G., 1990. The Velocity of Sound in Fluidized-Beds, Chemical Engineering Science 45(11), 3233-3245.

Ryzhkov, A. F., Tolmachev, E. M., 1983. Selection of optimal height for vibrofluidized bed, THEORETICAL FOUNDATIONS OF CHEMICAL ENGINEERING 17, 140-146.

Tsujimoto, H., Yokoyama, T., Huang, C. C., Sekiguchi, I., 2000. Monitoring particle fluidization in a fluidized bed granulator with an acoustic emission sensor, Powder Technology 113(1-2), 88-96.

van der Schaaf, J., Schouten, J. C., van den Bleek, C. M., 1998. Origin, propagation and attenuation of pressure waves in gas-solid fluidized beds, Powder Technology 95(3), 220-233.

Verloop, J., Heertjes, P. M., 1974. Periodic Pressure-Fluctuations in Fluidized-Beds, Chemical Engineering Science 29(4), 1035-1042.

Vervloet, D., Nijenhuis, J., van Ommen, J. R., 2010. Monitoring a lab-scale fluidized bed dryer: A comparison between pressure transducers, passive acoustic emissions and vibration measurements, Powder Technology 197(1-2), 36-48.

Wang, J. D., Cao, Y. J., Jiang, X. J., Yang, Y. R., 2009. Agglomeration Detection by Acoustic Emission (AE) Sensors in Fluidized Beds, Industrial & Engineering Chemistry Research 48(7), 3466-3473.

Wang, J. D., Ren, C. J., Yang, Y. R., 2010. Characterization of Flow Regime Transition and Particle Motion Using Acoustic Emission Measurement in a Gas-Solid Fluidized Bed, AICHE Journal 56(5), 1173-1183.

Appendix I: The flexibility matrix approach

The governing equation of the free vibrations of a linear undamped MDOF system for a normal-mode solution in the form $x = Xe^{iwt}$, where w is the frequency of vibration and X is the displacement vector (mode shape), after substitution read as:

$$-\omega^2 MX + KX = 0 \tag{17}$$

in which M is the mass matrix and K is the stiffness matrix. Under the assumption that the FB vessel structure has a positive MDOF stiffness matrix, eq. 5 can be written in terms of the flexibility matrix, A as:

$$\left(A \cdot M - \frac{1}{\omega^2} I \right) X = 0 \tag{18}$$

The solution to the computation of the natural frequencies of the systems reduced to solve the bracket term of eq. 18 and to compute the reciprocals of the positive squared roots of the eigenvalues of the AM product. As shown in eq. 18, although the physical construction and the motion itself were quite different between the transverse displacement and the translational problem, the definition and the properties of the elastic stiffness of the lumped mass were quite similar, in the sense that the dynamics of both systems can be represented by similar equations of motion. Within the flexural vibration problem, the elastic stiffness to the transverse deflection of the node masses was a function of the corresponding massless bending springs that interconnect them (de Silva, 2000).

According to the discrete model approach, the lumped masses, m_i, are of equal value and calculated as:

$$m_i = \frac{m_v}{\beta}; m = \rho_v A_{cv} L_c, i = 1, \ldots, n \left(\text{nodes}\right), \beta = n + 1 \tag{19}$$

The elements of the flexibility matrix, A, and the corresponding AM matrix are in the form:

$$f_{ij} = \frac{L_c^4}{EI} y_{ij} \Rightarrow AM = \phi \cdot y_{ij};\ \phi = \frac{\rho_v A_{cv} L_c^4}{EI} \tag{20}$$

where the y_{ij} are dimensionless flexibility coefficients, which can be determined as a function of the boundary conditions from the solution of the deflection of a beam subjected to concentrated loads (Kelly, 1993). The dimensionless natural frequencies, ω^*, are then obtained from the reciprocals of the positive squared roots of the eigenvalues of y_{ij} by considering the distributed inertia of the discrete approach:

$$\omega^* = \frac{1}{\sqrt{\beta \cdot \lambda}} \tag{21}$$

Finally, the dimensional natural frequencies are obtained as:

$$\omega_n = \frac{\omega^*}{\sqrt{\phi}} \Rightarrow \omega_n = \omega^* \cdot \sqrt{\frac{EI}{\rho_v A_{cv} L_c^4}} \tag{22}$$

Appendix II: Sequence of calculations.

The sequence of calculations followed by the program is sketched in Figure A.1. Initially, the bed pressure field was characterized to estimate both the number of nodes and the bed natural frequency used within the pulse-type functions. The natural frequencies characterizing the different modes of the structure were computed through the flexibility matrix approach (Appendix I). This information was further used to compute the damping coefficient matrix, C_n, according to the viscous damping model assumption. Finally, the transient response of the structure (eq. 12) was solved as a function of the forcing function. (i.e. vibration induced by a pulse excitation or a vibration induced by a pressure time series).

Figure Caption

Figure 1. Acoustic interaction model scheme: a) FB „zero' frequency model; b) stationary „resonance state' at f_n, and the resulting lumped mass structural approximation.

Figure 2. Simulated normalized time and frequency structural response of the Cylindrical UC3M vessel of table 2, pulse-type excitation runs for the fixed-fixed, pinned-pinned, fixed-pinned and fixed-fixed boundary conditions. The main expected frequency components present in the simulated signals are numbered in brackets.

Figure 3. Pulse-type induced excitation run for the UC3M vessel (table 2): a) Cumulative energy PSD function of the measured accelerometer signal; b) Normalized PSD of the measured accelerometer signal; c) Cumulative energy PSD function of the simulated accelerometer signals for fixed-free boundary conditions; d) Normalized PSD function of pulse-type excitation run accelerometer signals.

Figure 4 Concentrated load effects on the theoretical frequency and the time domain sinusoidal pulse-type excitation responses (Fixed-Free BC). The lower case *n* on the graphs accounts for the node position.

Figure 5. Distributed load effects on the theoretical frequency and the time domain sinusoidal pulse-type excitation responses (Fixed-Free BC). The lower case *n* on the graphs accounts for the node position

Figure 6. Comparison of the normalized PSD of the simulated pulse-type excitation run at Fixed-Fixed BC (dotted line) and the normalized PSD of the experimental accelerometer signal reported in the literature (Cody et al., 1996) (solid line) for an aluminum vessel operating with glass spheres of $d_p = 229\ \mu m$ fluidized with helium gas.

Figure 7. Comparison of the normalized PSD of the simulated pulse-type excitation runs (dotted line) for the boundary conditions a) Fixed-Free BC; b) Fixed-pinned BC; c)

pinned-pinned BC; and d) Fixed-Fixed BC as well as the normalized PSD of the experimental accelerometer signal reported in the literature (Jiang et al., 2007) (solid line) for a PMMA vessel operating with 0.5 kg of LLDPE of d_p = 360 μm. The red arrows point to the resonance frequency value of the accelerometer sensor used for the experimental run.

Figure 8. Comparison of the normalized PSD of the simulated pulse-type excitation runs (dotted line) using pinned-pinned BC. a) H/D = 2, d_p = 150 μm; b) H/D = 0.5, d_p = 280 μm; c) H/D = 1, d_p = 280 μm; and d) H/D = 2, d_p = 280 μm as well as the normalized PSD of the experimental accelerometer signal reported in the literature (Abbasi et al., 2009) (solid line) for a PMMA circulating vessel operating with sand particles. The red arrows point to the main resonance frequency peaks value detected in both cases.

Figure 9. Time domain comparison between the measured and the induced responses by pressure time series accelerometer signals for the UC3M PMMA vessel (table 2). a) 30 seconds of dynamics (please note the beating phenomena on both measured and simulated time series); b) the detail of the time domain structure (t_m t_e) of the measured and the simulated accelerometry signals.

Figure 10. Comparison of the normalized PSD of the simulated pressure-type excitation run (black line) at Fixed-Free BC and the normalized PSD of the experimental accelerometer signal measured at the UC3M PMMA vessel (table 2). a) PSD function comparison; b) Cumulative PSD energy function.

Figure 11. PSD of the measured pressure time series (solid red line) and the envelope signals extracted from: measured accelerometer signals (dotted red line); simulation accelerometer signals (dotted black line).

Figure A1. Sequence of calculations

Table caption

Table 1. Pulse-type functions and transient response conditions

Table 2. Experimental condition used through the simulations. The * superscript symbol accounts for the assumed values.

Figure 1

Click here to download high resolution image

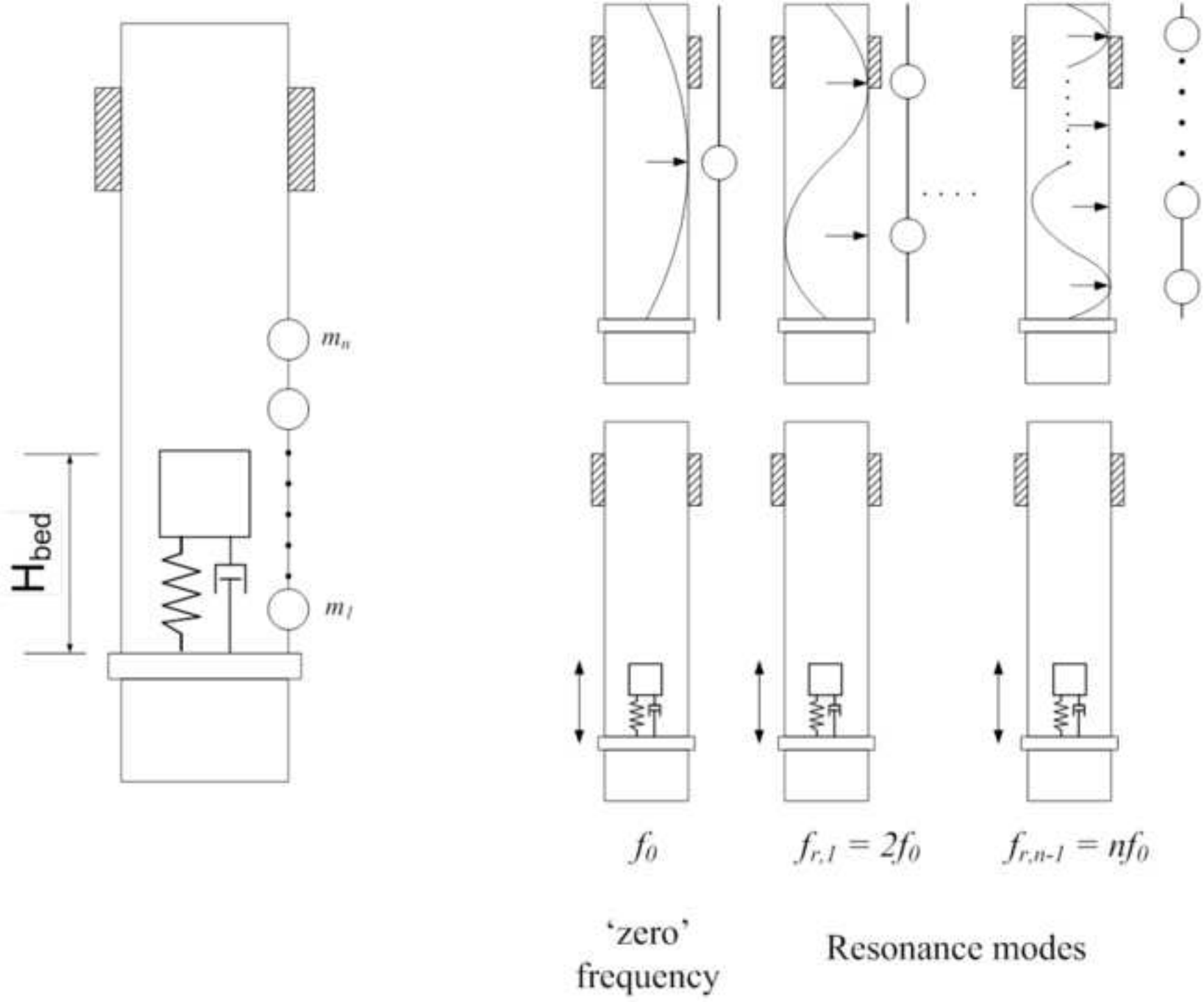

Figure 2

Click here to download high resolution image

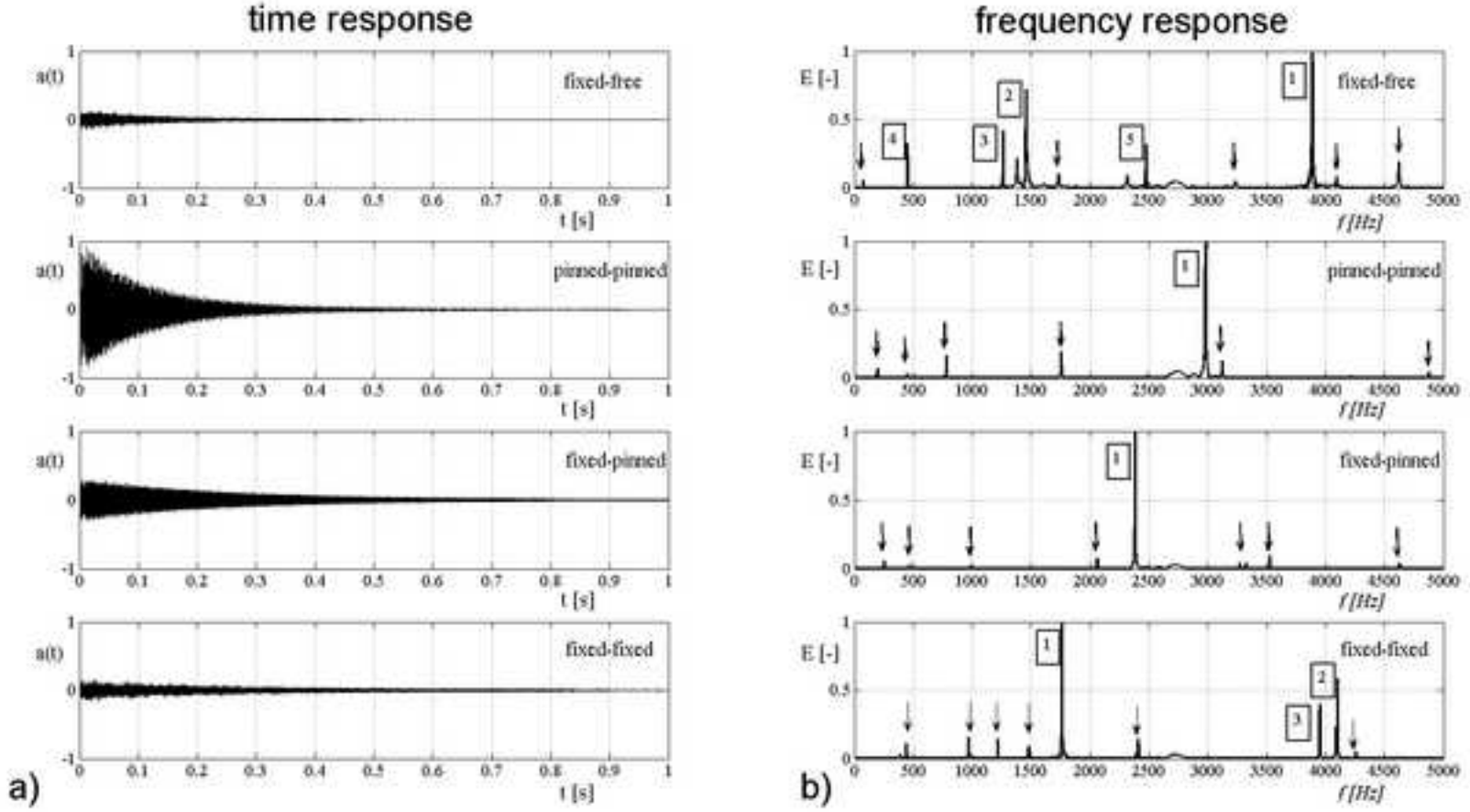

Figure 3

Click here to download high resolution image

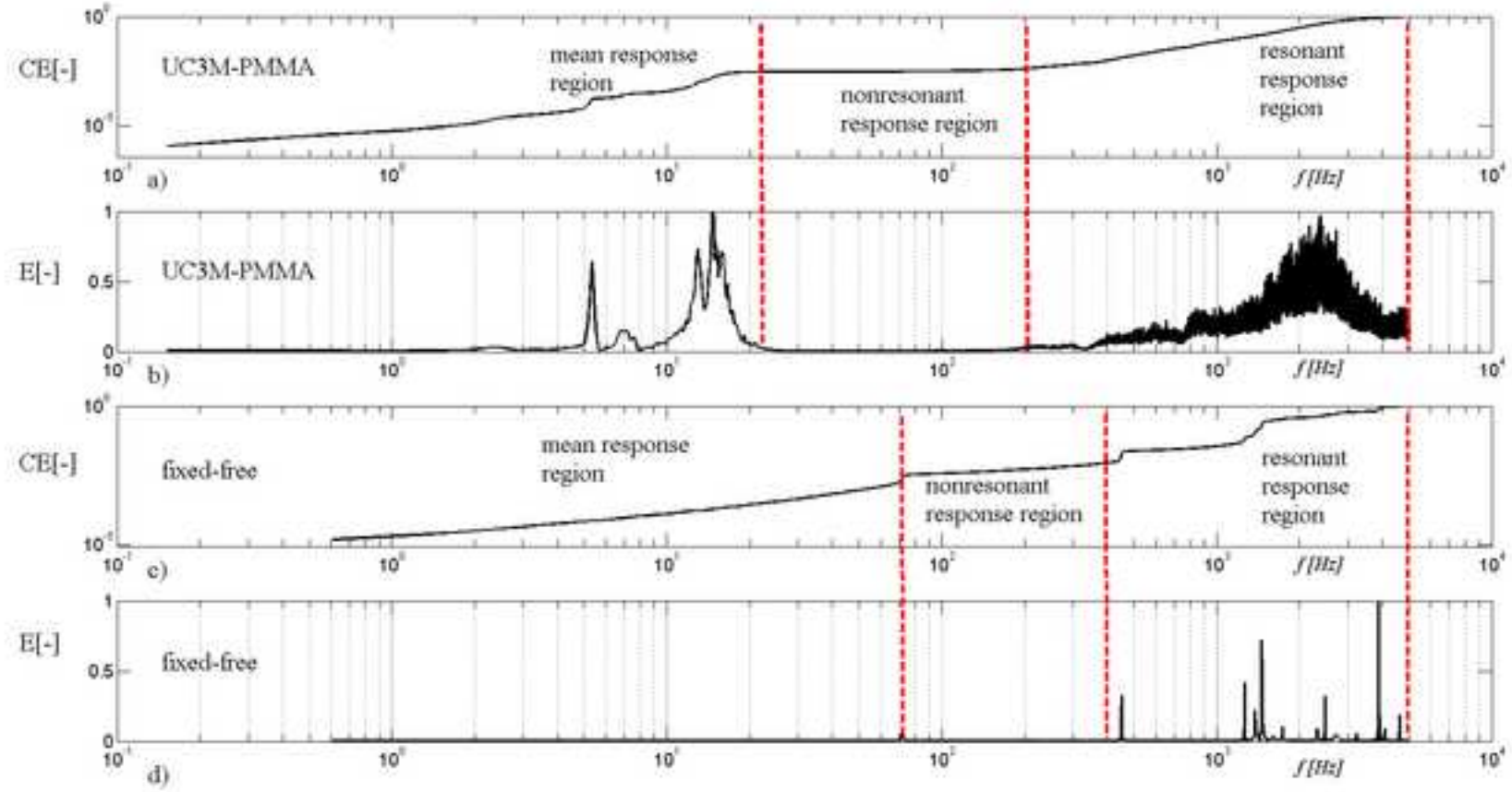

Figure 4

Click here to download high resolution image

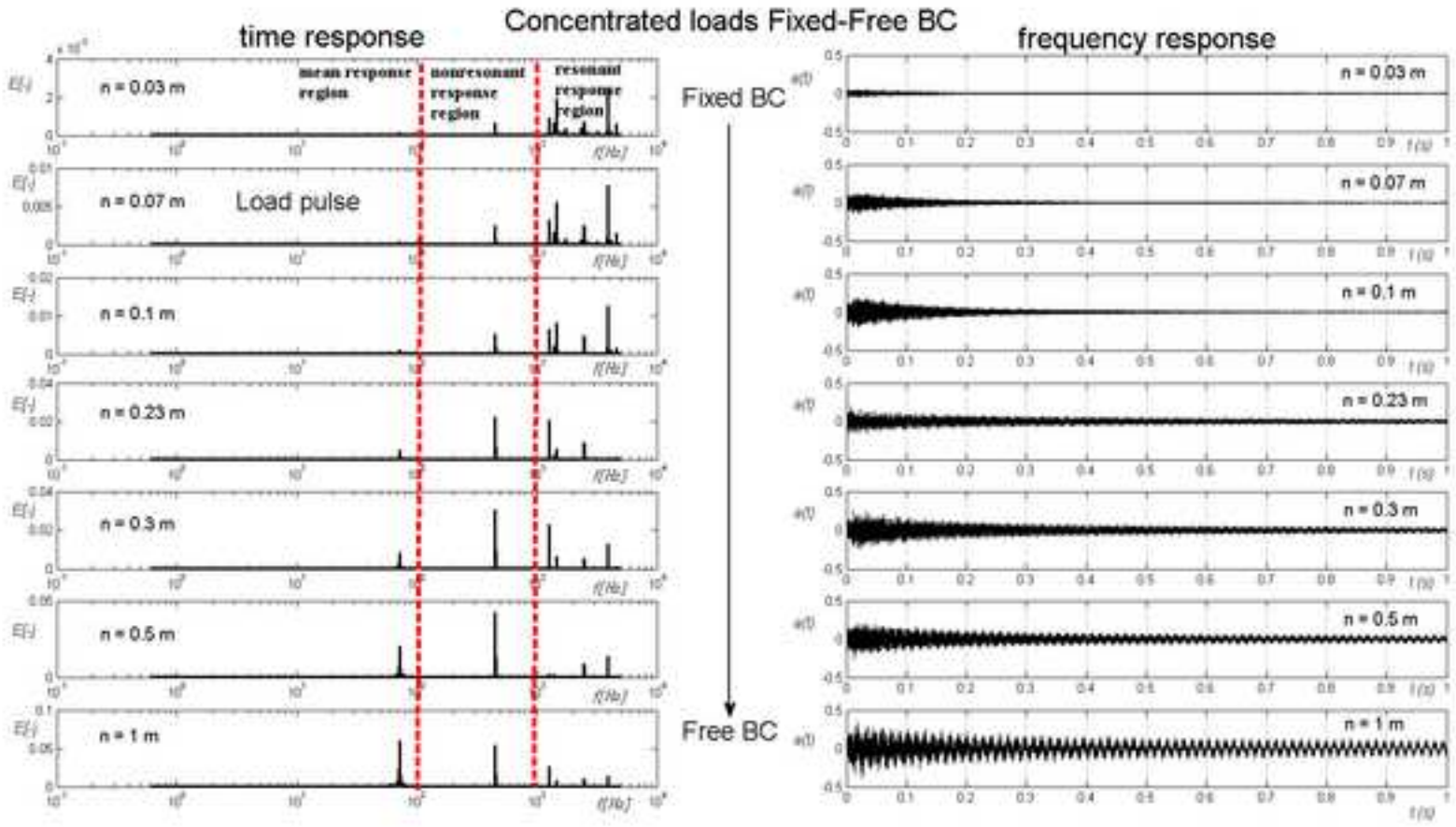

Figure 5

Click here to download high resolution image

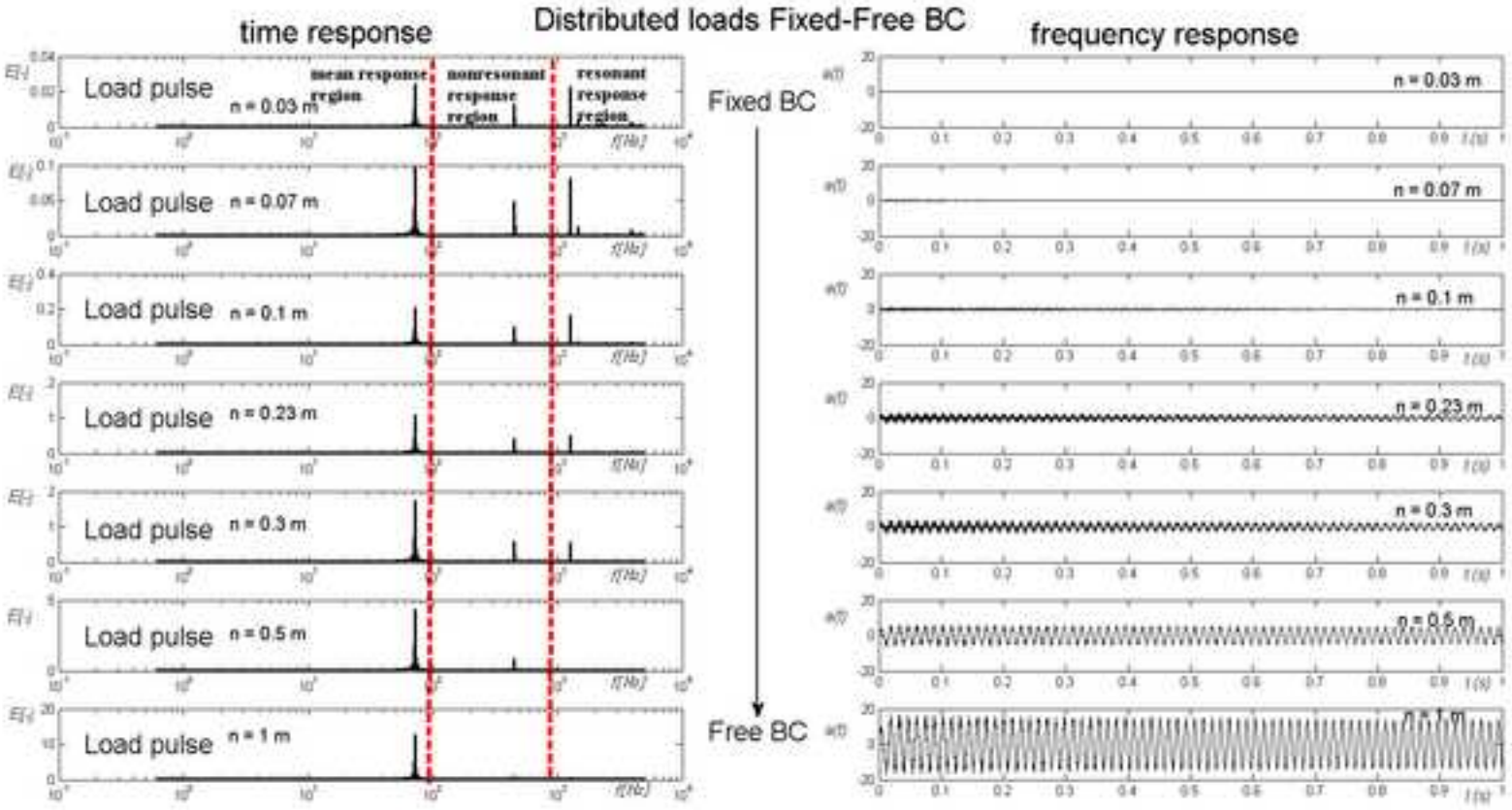

Figure 6

Click here to download high resolution image

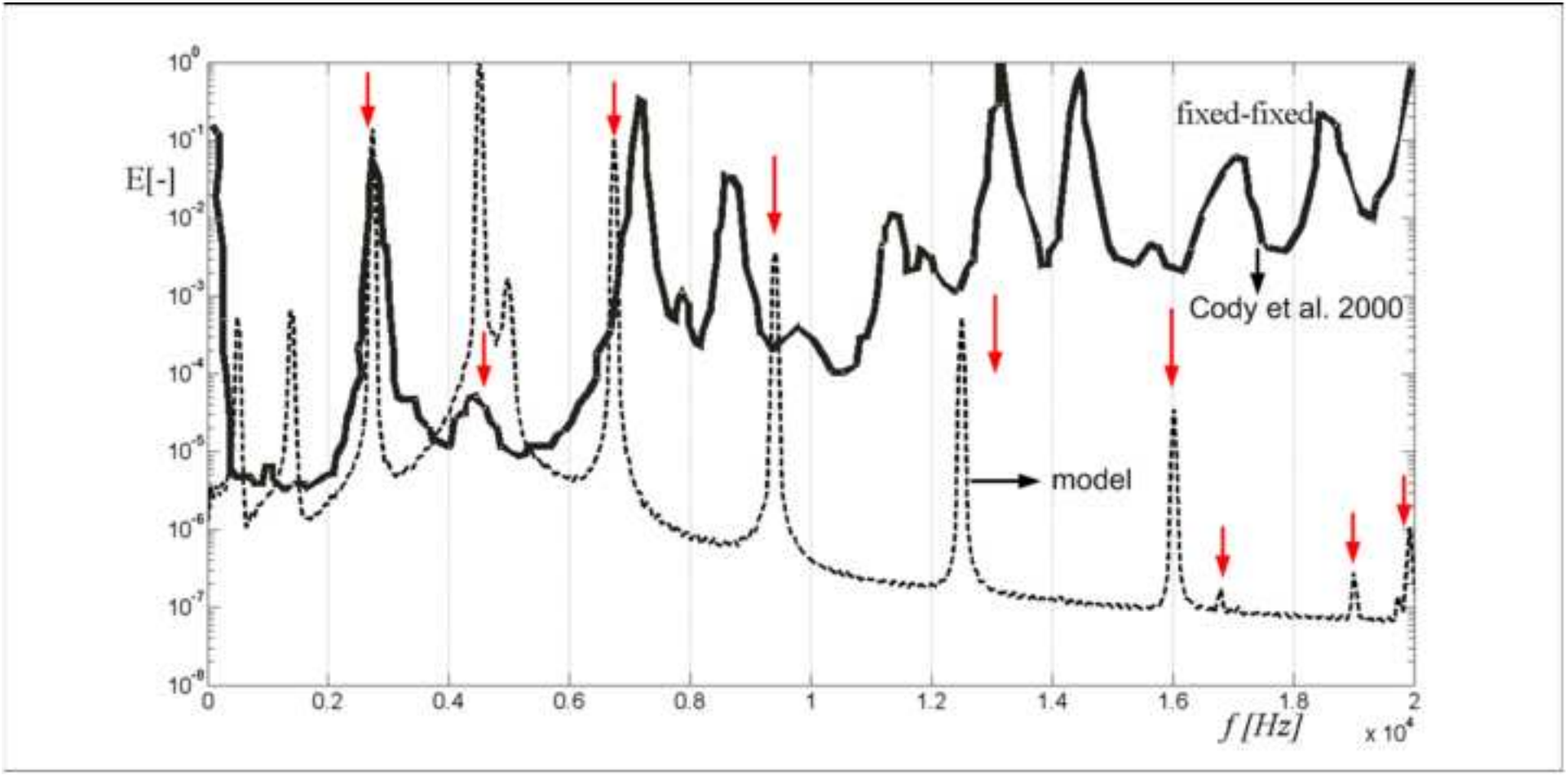

Figure 7
Click here to download high resolution image

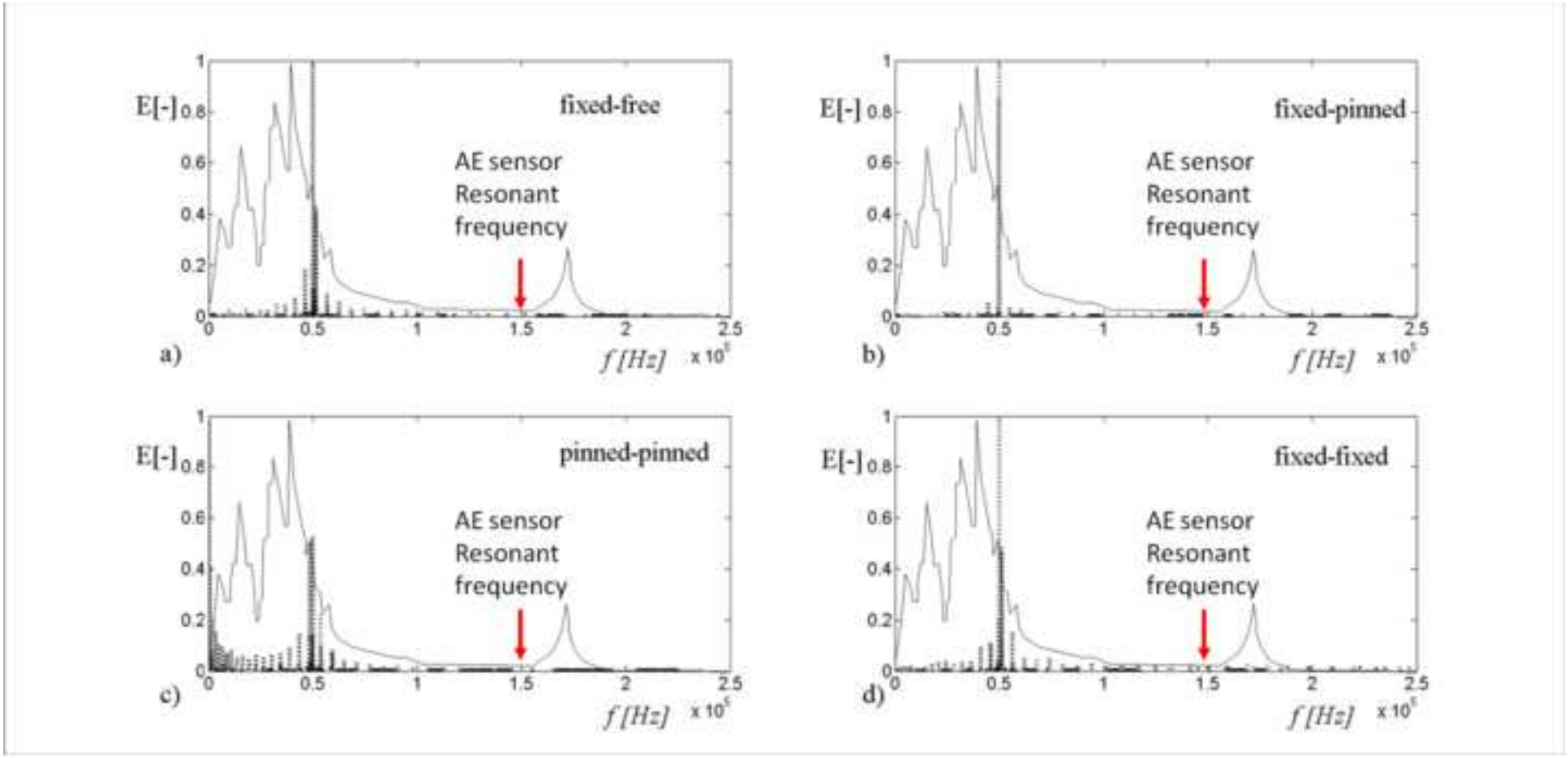

Figure 8

Click here to download high resolution image

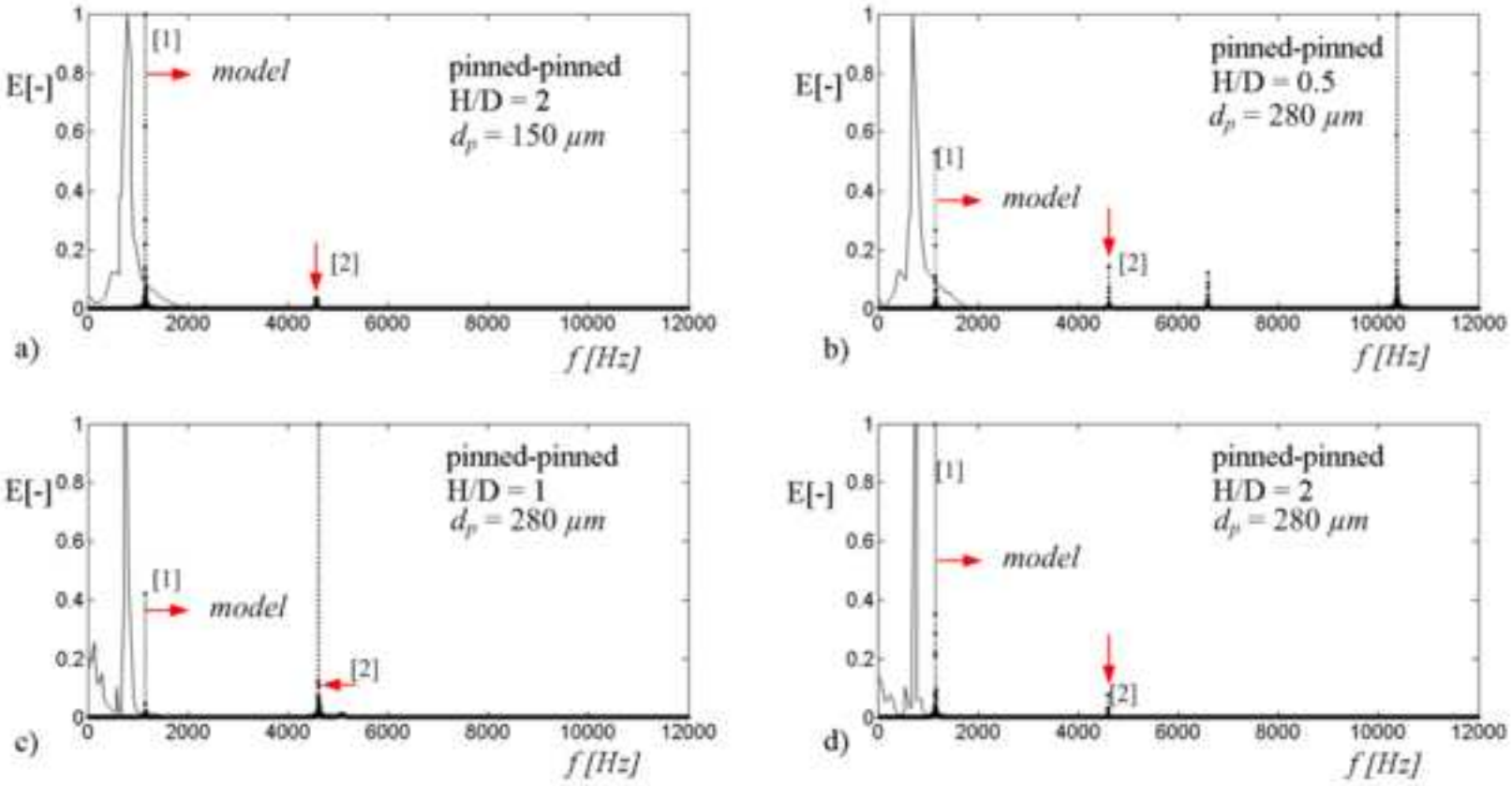

Figure 9

Click here to download high resolution image

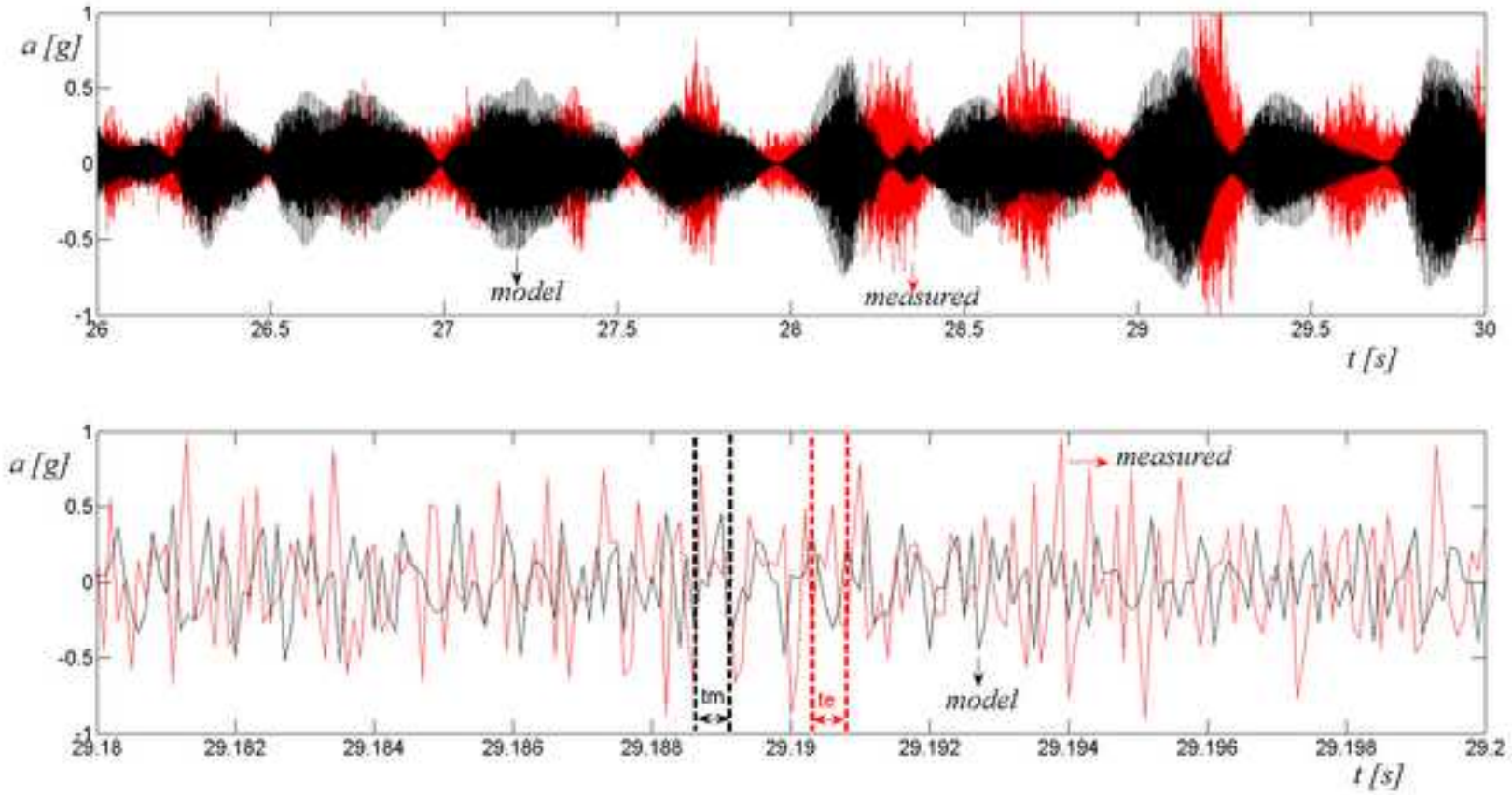

Figure 10
Click here to download high resolution image

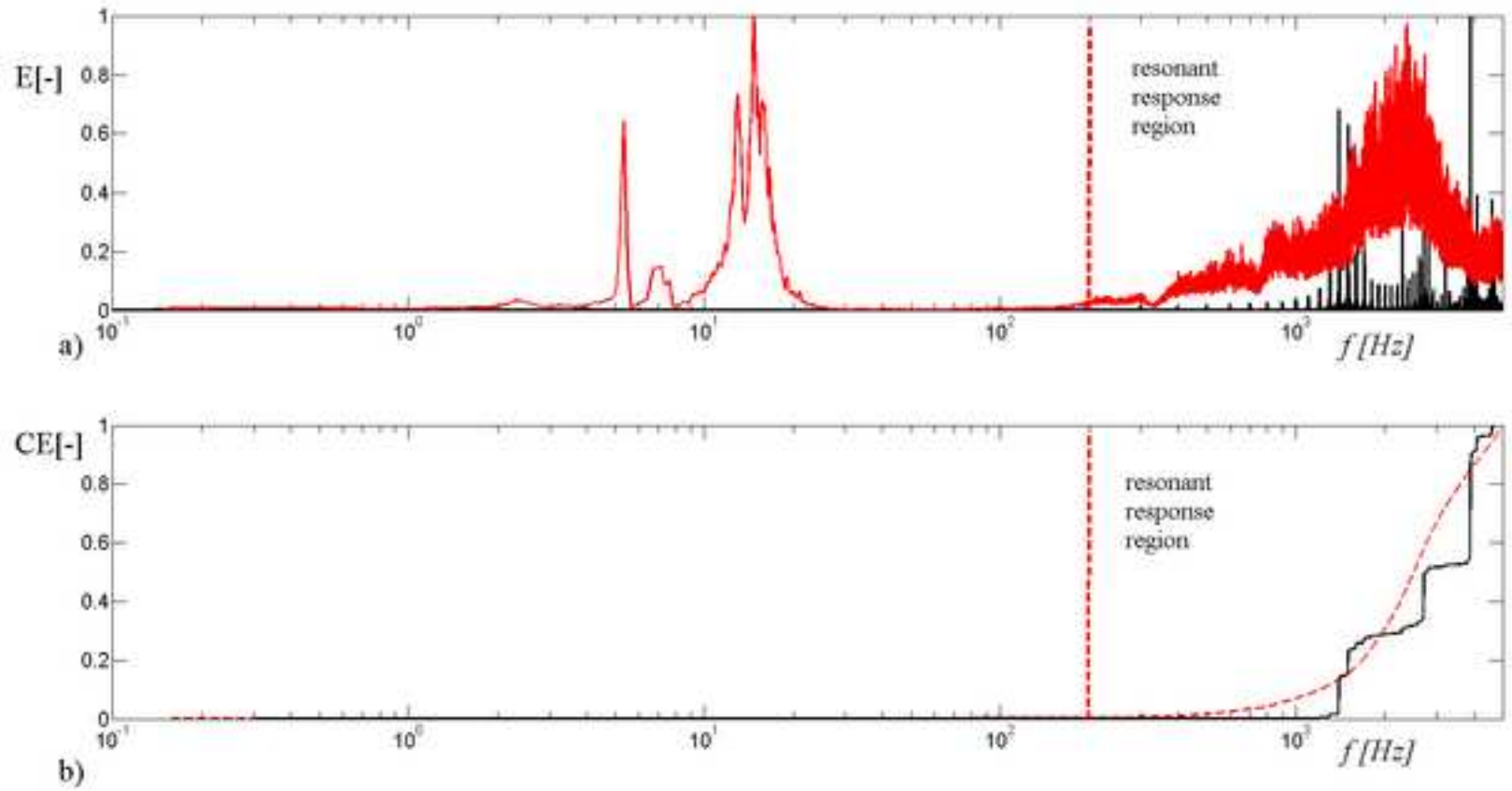

Figure 11

Click here to download high resolution image

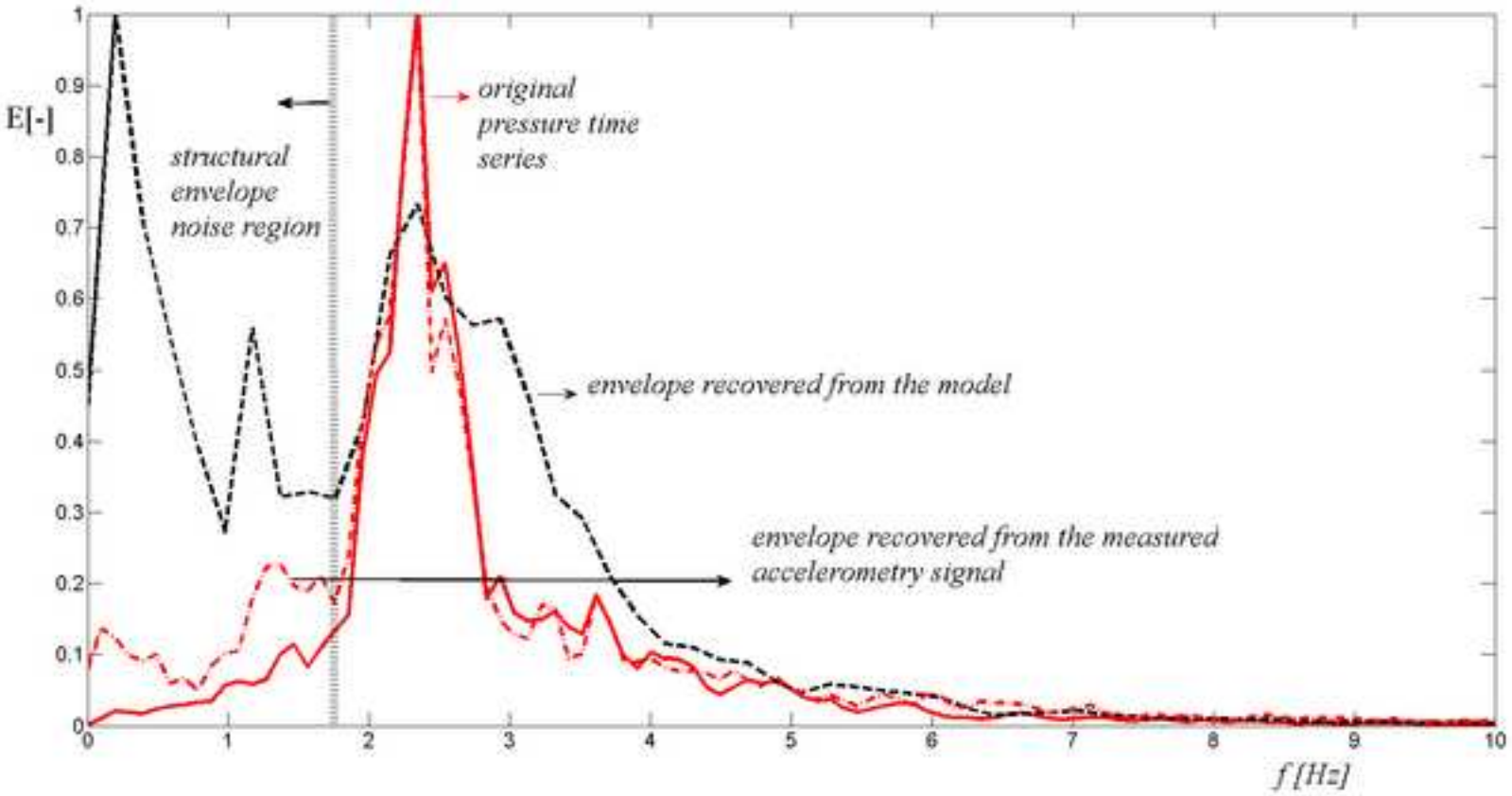

Figure
Click here to download high resolution image

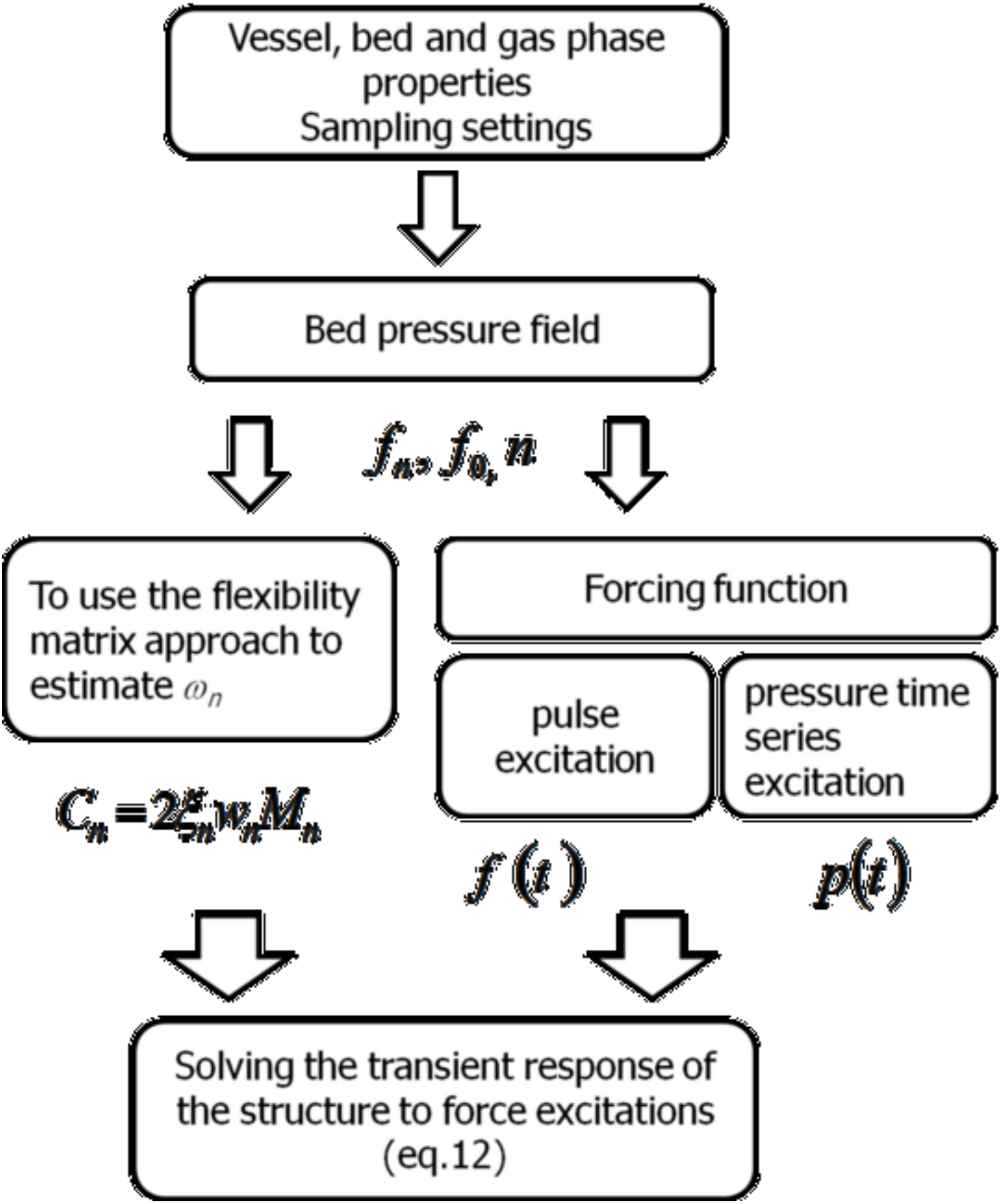

Table

Click here to download Table: tablesv2R1.doc

Pulse-type	**Forcing function**	**Rise time, t_0, s**	**Force magnitude, F_0**	**Boundary conditions**
Impulse	$f(t) = F_0$	$1 \cdot 10^{-3}$ - $1 \cdot 10^{-2}$	$F_0 = m_{bulk}\ddot{x} = m_{bulk} C \cdot w_{bed}^2$, $m_{bulk} = \left[\rho_p(1-\varepsilon) + \rho_g \varepsilon\right] A_{bed} H_{bed}$ $C = \lambda / n$ $w = 2\pi f_n$	fixed-free pinned-pinned fixed-pinned fixed-fixed
Exponential decay	$f(t) = F_0 e^{[-\alpha(t-t_0)]}$, α = 0.5 s^{-1}			
Sinusoidal	$f(t) = F_0 \left[1 - \cos^2\left(\frac{w_{bed} t}{t_0}\right)\right]$			
Sinusoidal + exponential decay	$f(t) = F_0 \left[\left[1 - \cos^2\left(\frac{w_{bed} t}{t_0}\right)\right] + e^{[-\alpha(t-t_0)]}\right]$			

Table 1. Pulse type functions and transient response conditions

	Vessel properties					*Bed & material characteristics*					*Gas phase*				*Sampling settings*
Unit	Geometry & distributor type	size [m]	E, GPa	ρ, kg/m^3	L, m	H [m]	d_p [μm]	ρ_p [kg/m^3]	ε_{mf}	ϕ_s	gas	μ, 10^5, $Pa \cdot s$	ρ_g [kg/m^3]	γ	f_s, kHz
Cody et.al (1996) (Aluminium vessel)	Cylindrical / perforate plate	0.0762 (ID) 0.0826(OD)	68.9	2700	0.26	0.16	297	2640	0.43	0.9	Helium	1.86	0.1785	1.664	50
Jian et al. (2007) (PMMA vessel)	Cylindrical / perforate plate	0.15 (ID) 0.154*(OD)	3*	1190	1	0.05	360 (LLDPE)	920	0.43	0.9*	Air	1.85	1.2	1.4	500
Abassi et al. (2009) (PMMA vessel)	Cylindrical / perforate plate	0.15 (ID) 0.154*(OD)	1.8·/ 3.9	1190	2	0.075 0.15 0.225	150 280 (sand)	2640	0.43	0.86*	Air	1.85	1.2	1.4	25
UC3M (PMMA Vessel)	Cylindrical / perforate plate	0.192 (ID) 0.196 (OD)	1.8 / 3.9	1190	1	0.14	637 (sand)	2632		0.86*	Air	1.85	1.2	1.4	10

Table 2. Experimental condition used through the simulations. The * superscript symbol accounts for assumed values.

Supplementary Material

Click here to download Supplementary Material: DSC_0301.JPG